UNIVERSITÀ
DI PAVIA

PhD IN BIOMEDICAL SCIENCES
DEPARTMENT OF BRAIN AND BEHAVIORAL SCIENCES
UNIT OF NEUROPHYSIOLOGY

Comparison of vestibular and cochlear hair cells currents from wild-type and $Ca_v1.3^{-/-}$ mice

PhD Tutor: Prof. *Giancarlo Russo*

PhD dissertation of
Roberta Giunta

a.a. 2020/2021

Index

The ear anatomy 1
Outer ear 1
Middle ear 2
Inner ear 3
The Cochlear Apparatus 4
Auditory Function 5
Auditory Projection 6
The Vestibular Apparatus 8
The Semicircular Ducts 8
Otholitic Organs 9
Vestibular Projection 11
Hair cells 13
Cochlear hair cells 15
Vestibular hair cells 17
Ribbon Synapse 19
Mechano-electric transduction 21
Voltage-dependent K^+ channel in Vestibular hair cells 25
Voltage-dependent Ca^{2+} channel in Cochlear hair cells 27
Voltage-dependent Ca^{2+}channel in Vestibular hair cells 29
Glutamate exocytosis in cochlear and vestibular hair cells 30
Introduction 32
Experimental investigation 34
Materials and Methods 34
Tissue preparation 34
Whole-cell electrophysiology 35
Data analysis 36
Results 37
Potassium currents recorded from Type I and Type II crista hair cells from control and $Ca_v1.3^{-/-}$ mice 37
Calcium currents in Type I and Type II hair cells in control and $Ca_v1.3^{-/-}$ mice 40
Calcium currents in the Inner Hair Cells (IHCs) of the mouse cochlea from $Ca_v1.3^{-/-}$ mice 47
Discussion 49
References 51
Sitography 66

The ear anatomy

The ear consists of three sections named outer, middle, and inner ear (Fig.1). The outer and the middle ear are able to conduct sound to the inner ear, where vibration is converted to nerve signals.

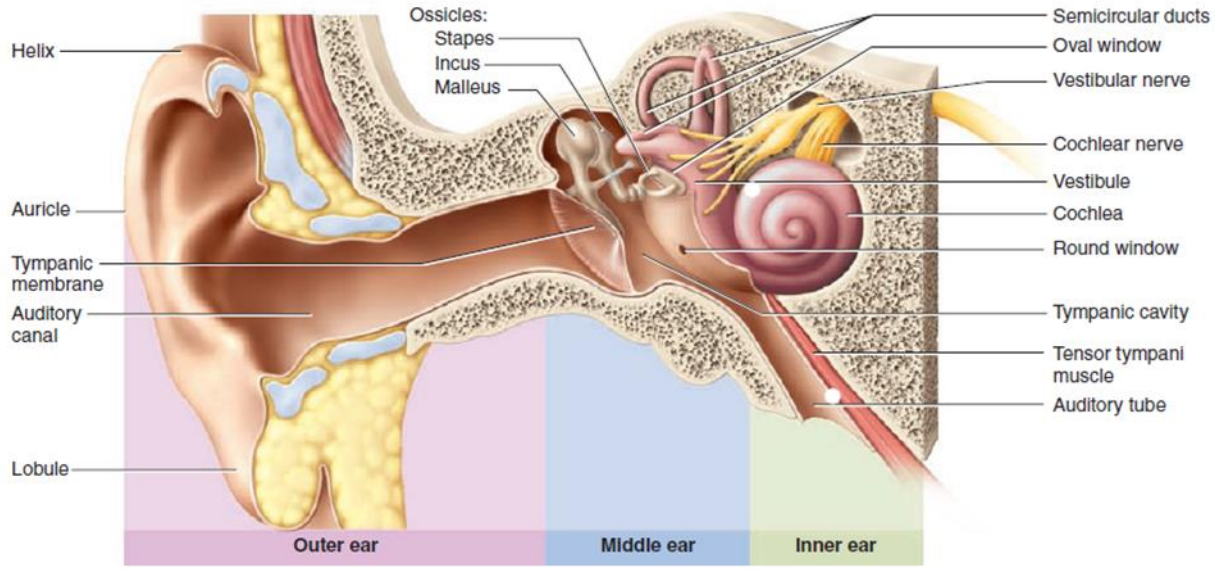

Figure 1. Internal Anatomy of the Ear. Human Anatomy. Kenneth S. Saladin, 2017.

Outer ear

The outer ear conducts airbone vibrations to the tympanic membrane (eardrum). It is composed by auricle or pinna, made up of the elastic cartilage except for the earlobe, which is mostly adipose tissue. The auricle consists of the helix, arrangement of whorls, that directs sound into the auditory canal.

The auditory canal or auditory *meatus* is the passage through the temporal bone. It follows a S-shaped course for about 3 cm to the tympanic membrane. It is covered by the skin and supported by fibrocartilage (near the auricle) in the first part and by the temporal bone in the second part (near the tympanic membrane). The sound waves propagating through the *meatus* cause the tympanic membrane to vibrate.

Middle ear

The middle ear consists of the tympanic cavity of the temporal bone. A space located between the outer and the inner ears, it houses three smallest bones and two skeletal muscles.

The middle ear begins with the tympanic membrane or eardrum which separates the auditory canal from the middle ear.

This membrane is suspended in the temporal bone and vibrates in response to sound, moreover it is innervated by the nerve fibers of the vagus and the trigeminal and is highly sensitive to pain. Posteriorly, the tympanic cavity is continuous with the mastoid process. The cavity is filled with air that enters by way of the auditory (pharyngotympanic) tube**,** a passage to the nasopharynx.

Swallowing or yawning opens the auditory tube and allows air to enter or leave the tympanic cavity. This equalizes air pressure on both sides of the tympanic membrane, allowing it to vibrate freely.

The three auditory ossicles of the tympanic cavity are the *malleus*, the *incus*, and the *stapes* (Fig.1).

The first has a handle attached to the inner surface of the tympanic membrane and a short process, which articulates with the *incus*. The *incus* has a triangular body that meets the *malleus* and a long *limb* that articulates with the *stapes*.

The *stapes* has a head that articulates with the *incus* and her base lies on the oval window, where the inner ear begins.

The muscles of the middle ear are the *stapedius* and *tensor tympani*. The *stapedius* arises from the posterior wall of the cavity and inserts on the *stapes*. The *tensor tympani* travels the auditory tube and inserts on the *malleus*. In response to loud noises, these muscles contract and dampen the vibration of the ossicles, thus protecting the sensory cells of the inner ear; this is called the tympanic reflex (Kenneth S. Saladin, 2017).

Inner ear

The inner ear is located within the bony labyrinth in the petrous part of the temporal bone. The bony labyrinth contains a complex of fluid-filled chambers and tubes called the membranous labyrinth. (Fig.2) (Kenneth S. Saladin, 2017).

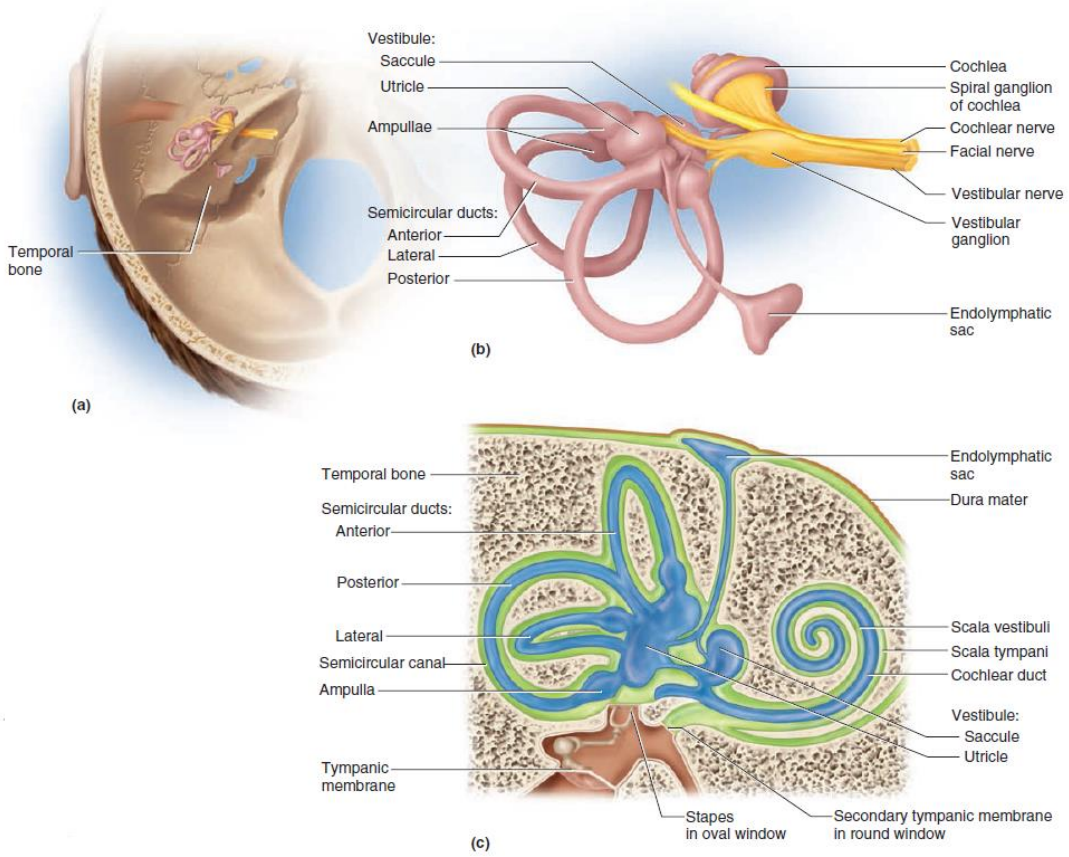

Figure 2. Anatomy of the Membranous Labyrinth. (a) Position and orientation within the petrous part of the temporal bone. (b) Structure of the membranous labyrinth and its nerve. (c) Relationship of the perilymph (green) and endolymph (blue) to the membranous labyrinth. Human Anatomy. Kenneth S. Saladin, 2017.

The fluid in this labyrinth, called endolymph is like intracellular fluid in fact it is rich in K^+ (150 mM) and low in Na^+ (1 mM) and Ca^{2+} (20 μM) (Pickels, 2008).

Between the membranous labyrinth and bone is another liquid, like cerebrospinal fluid, called perilymph. The perilymph is an extracellular fluid rich in Na^+ (140 mM) and low in K^+ (4-5 mM) (Bernard et al., 1986).

The difference in composition, between endolymph and perilymph, allows the K^+ transducer current to flow from the endolymphatic compartment to the perilymphatic compartment (Davis, 1965).

The inner ear consists of cochlea and vestibule (Fig.2b). The cochlea converts sound pressure patterns from the outer and middle ear into electrochemical impulses, which travel to the brain via the auditory nerve. Instead, the vestibule, which is characterized by three semicircular canals (SCCs) and two otolith organs (utricle and saccule), is the structure dedicated to balancing. It converts head movements into electrochemical impulses which are passed on to the brain through the vestibular nerve.

The Cochlear Apparatus

The cochlea named for its snail-like shape is a structure dedicated to hearing. It contains the organ of hearing, called the cochlear duct (Fig.3a, b). The cochlear duct appears as a triangular space bounded by a basilar membrane below and a vestibular membrane above. Above the vestibular membrane is a space called the *scala vestibuli*, and below the basilar membrane is a space called the *scala tympani* (Fig. 3b). These spaces are filled with perilymph and communicate with each other through a narrow channel at the apex of the cochlea. The *scala vestibuli* begins near the oval window and spirals to the apex; from there, the *scala tympani* spirals back down to the base and ends at the round window (Fig.3b) (Kenneth S. Saladin, 2017).

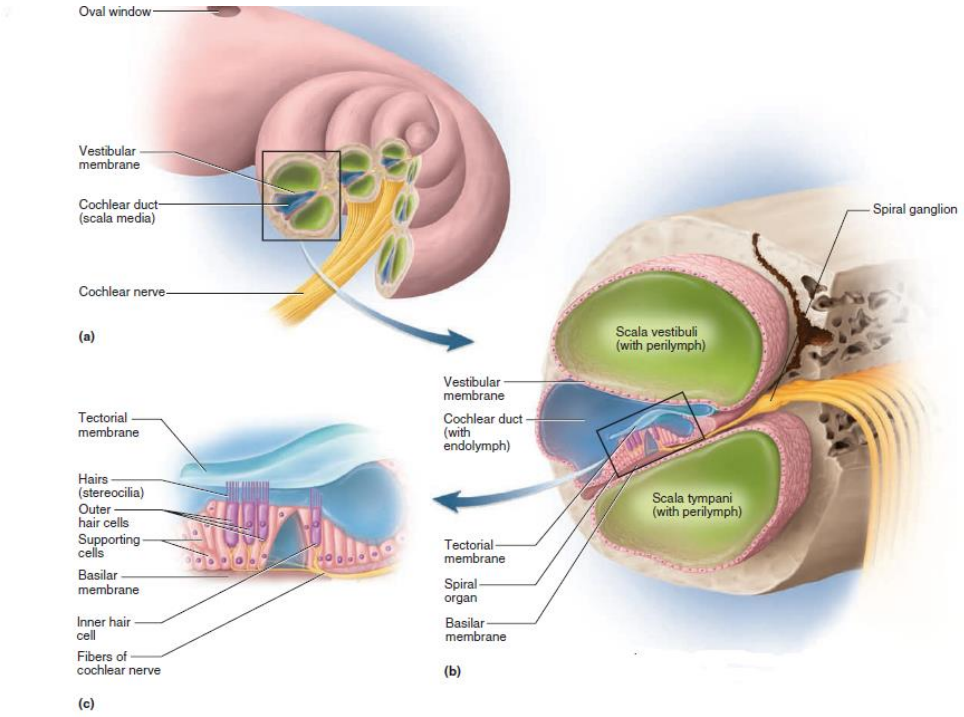

Figure 3. Anatomy of the Cochlea. (a) Vertical section. (b) Details of one section through the Cochlea. (c) Details of the spiral organ epithelium. Human Anatomy. Kenneth S. Saladin, 2017.

On the basilar membrane of the cochlear duct is located the spiral organ or Organ of Corti which contains the sensory receptor cells, known as hair cells and supported cells.

There are two groups of hair cells (Fig.3c): the Inner Hair Cells (IHCs), are arranged in a single row and the outer hair (OHCs) cells, are arranged in three rows. At the apical tip of each hair cell is a hair bundle, consisting of 40–80 *stereocilia* and a *kinocilium*, the latter located at the tallest site of the bundle that is made up of two central fibrils surrounded by nine double fibrils (Marcotti and Masetto, 2010). At their basal ends, inner and outer hair cells synapse with both first-order sensory neurons and motor neurons from the cochlear branch of the vestibulocochlear (VIII) nerve (Gerard J. Tortora and Mark T. Nielsen, 2017).

The geometry of the organ of Corti and the disposition of the tectorial membrane, ensure that when the basilar membrane vibrates it causes lateral deflection of the mechanosensory hair bundles. (Petit and Richardson, 2009; Schwander et al., 2010). This deflection opens mechanosensitive ion channels that carry a depolarizing inward current, which generates sustained and graded receptor potentials within the hair cells (Marcotti W, 2012).

Auditory Function

When sound waves strike the tympanic membrane, this vibration is transmitted from the *malleus* to the *incus* and then to the *stapes*.

As the *stapes* moves, its oval-shaped footplate, causes the oval window to vibrate. As the oval window bulges inward, it pushes on the perilymph of the *scala vestibuli*.

Pressure waves are transmitted from the *scala vestibuli* to the *scala tympani* and to the round window, causing it to bulge outward into the middle ear. When the pressure waves travel through the *scala vestibuli*, then move into the endolymph inside the cochlear duct (Fig.4). The pressure waves in the endolymph cause the basilar membrane to vibrate, which moves the hair cells of the spiral organ against the tectorial membrane. Each upward movement of the hair cells crowds the *stereocilia* against the tectorial membrane, forcing them to rock back and forth. This motion opens Mechano-Electrical Transducer (MET) channels express on the hair bundle, that admit bursts of potassium ions into the hair cells, exciting the cells. An excited hair cell releases a neurotransmitter from synaptic vesicles in its base, and this leads to the generation of nerve impulses in first-order neurons in cochlear nerve fibers.

Each segment of the basilar membrane is tuned for a particular pitch. High-pitched sounds especially stimulate hair cells near the base of the cochlea, and low-pitched sounds stimulate those near the tip. Thus, the brain distinguishes loudness and pitch from how fast the cochlear

nerve fibers are firing and what regions of the spiral organ are generating the strongest signals (Kenneth S. Saladin, 2017; Gerard J. Tortora and Mark T. Nielsen, 2017).

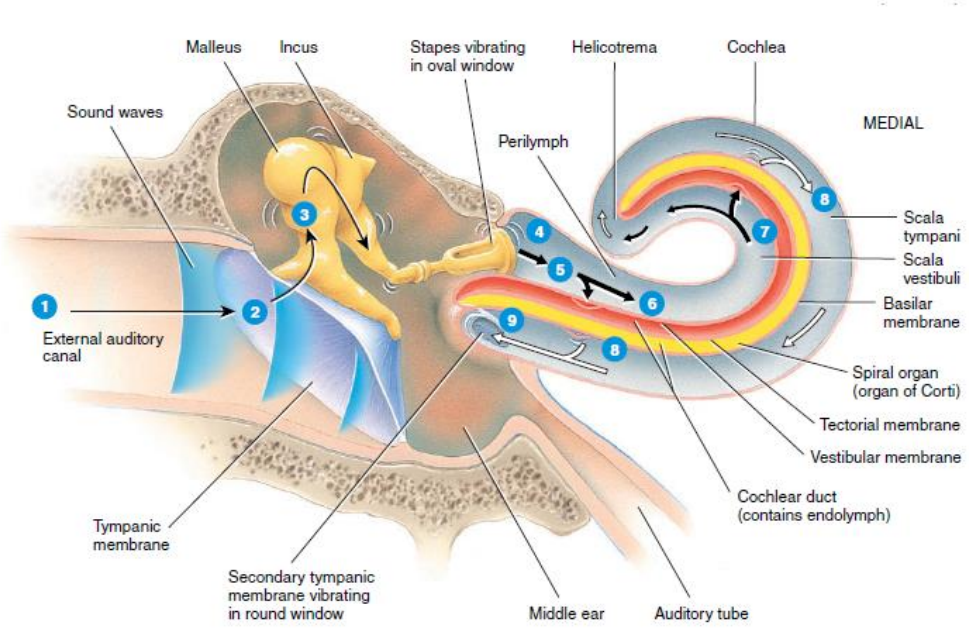

Figure 4. The basic mechanisms of the auditory function. Gerard J. Tortora and Mark T. Nielsen, 2017.

Auditory Projection

Sensory nerve fibers from the cochlea, together with vestibular nerve become the vestibulocochlear nerve.

The vestibulocochlear nerve leaves the inner ear and enters the cranial cavity, specifically in the cochlear nucleus of the *medulla oblongata*. Cochlear nerve fibers synapse here with second-order neurons that lead to the superior olivary nucleus of the *pons*. From this region, this nucleus sends signals back to the outer hair cells tugging on the basilar and tectorial membranes for the purpose to suppress the vibration of specific regions of the basilar membrane. This enhances the ability of the brain to tell one sound frequency from another, an important skill to distinguish the words in someone else's speech.

Moreover, the superior olivary nucleus of the *pons* sends signals to the *tensor tympani* and stapedius muscles, which are responsible for the tympanic reflex and compares signals from the right and left ears to identify the direction from which sound is coming.

Other connections from the *pons* reaches the *inferior colliculi* of the midbrain. It issues fibers to the thalamus. In the thalamus, these fibers synapse with neurons that continue to the primary auditory cortex in the superior part of each temporal lobe (Fig.5). The temporal lobe is the site

of conscious perception of sound; for example, the ability to recognize what a sound is, occurs in the auditory association area bordering the primary auditory cortex.

The auditory cortex on each side of the brain receives signals from both ears. Because of this extensive decussation, damage to the right or left auditory cortex does not cause a unilateral loss of hearing (Kenneth S. Saladin, 2017).

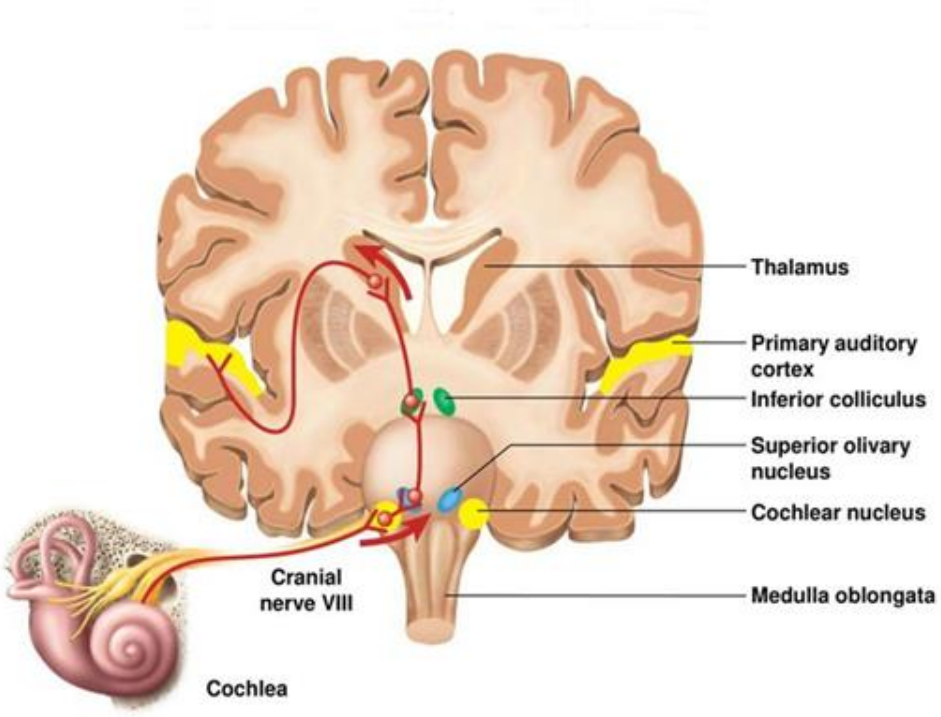

Figure 5. The Auditory Projection Pathway. (https://images.app.goo.gl/C7i98SyvYN3bwp4V8).

The Vestibular Apparatus

The original function of the ear in vertebrate history was not hearing, but balance, and spatial orientation.
It is composed of three semicircular ducts and two otolithic organ composed by saccule and utricle.
The semicircular ducts are responsible for dynamic equilibrium, the perceptions of the head movements or angular accelerations, instead the saccule and utricle for static equilibrium, the perception of the orientation of the head or linear accelerations related to gravity (Goldberg JM and Fernández C, 1975).

The Semicircular Ducts

The semicircular Canals (SCCs) are curved ducts, connected to the utricle, they respond to angular accelerations or rotation of the head. The three SCCs are anterior, posterior, and horizontal. The orientation of the ducts causes each different duct to be stimulated by rotation of the head in different planes. Each duct is filled with endolymph and has a sac called *ampulla*. Within the ampulla is a pile of hair cells and supporting cells called *crista ampullaris*. The hair cells have *stereocilia* and a *kinocilium* embedded in the *cupula* a gelatinous membrane that extends from the *crista* to the roof of the *ampulla*. Each SCC works together with a SCC on the other side of the head, and it means that SCCs are paired as follows: right anterior with left posterior, left anterior with right posterior, left lateral with right lateral. For this reason, each canal can detect angular acceleration in its specific plane; this arrangement allows for a 3-dimensional vector representation of rotational acceleration. When the head turns, the duct rotates, but the endolymph lags behind and pushes the cupula in the opposite direction of the head direction (Fig.6). This bends the *stereocilia* and stimulates (or inhibits) the hair cells. When the rotational velocity of the head becomes constant, the *cupula* returns to its upright position because of its elastic structure. Rotational deceleration of the head results in cupula displacement in the same direction as the head movement (Khan and Chang, 2013).

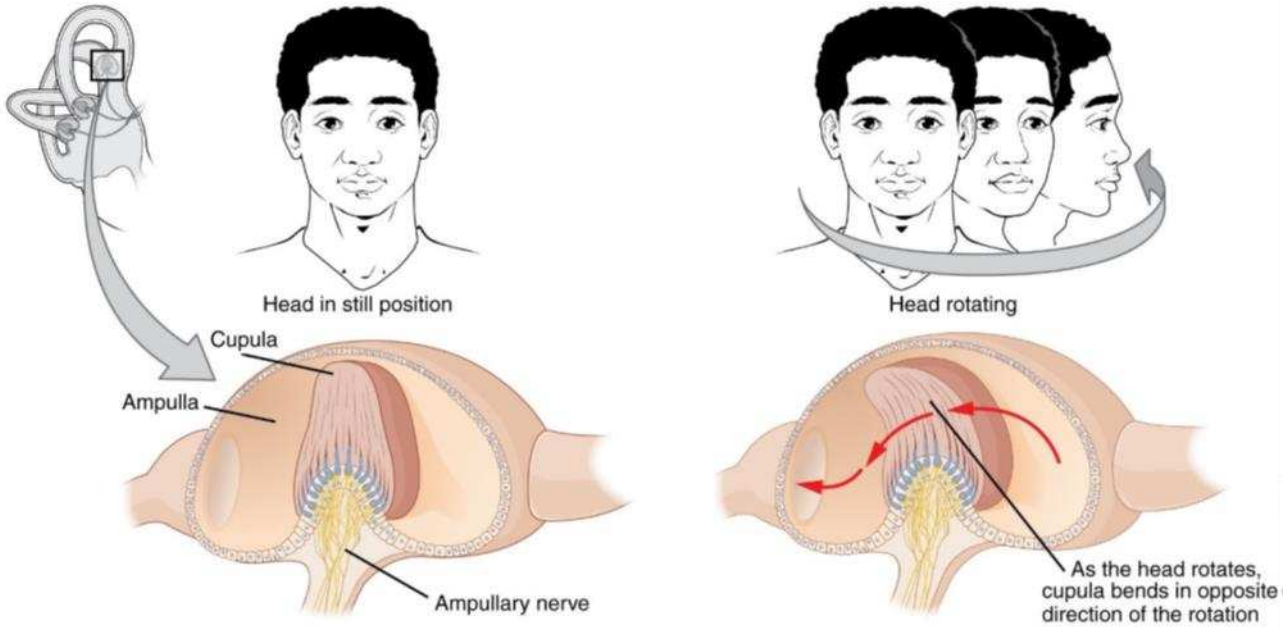

Figure 6. SCCs have the task of detect rotational movement of the head. As one of the canals moves in an arc with the head, the endolymph moves in the opposite direction, causing the cupula and stereocilia to bend. (https://open.oregonstate.education/aandp/chapter/15-4-equilibrium/).

Otholitic Organs

The saccule and the utricle are known as otolithic organs which contain a sensory epithelium, the *macula*, consisting of sensory cells, the hair cells, and supporting cells. Overlying the hair cells and their hair bundles is a gelatinous layer, the otolithic membrane, which is fibers structure and embedded with crystal of carbonate, called *otoconia*.

The otolithic membranes of saccule and utricle differ for membrane thickness and size of otoliths (Fig.7) (Lindeman, 1973).

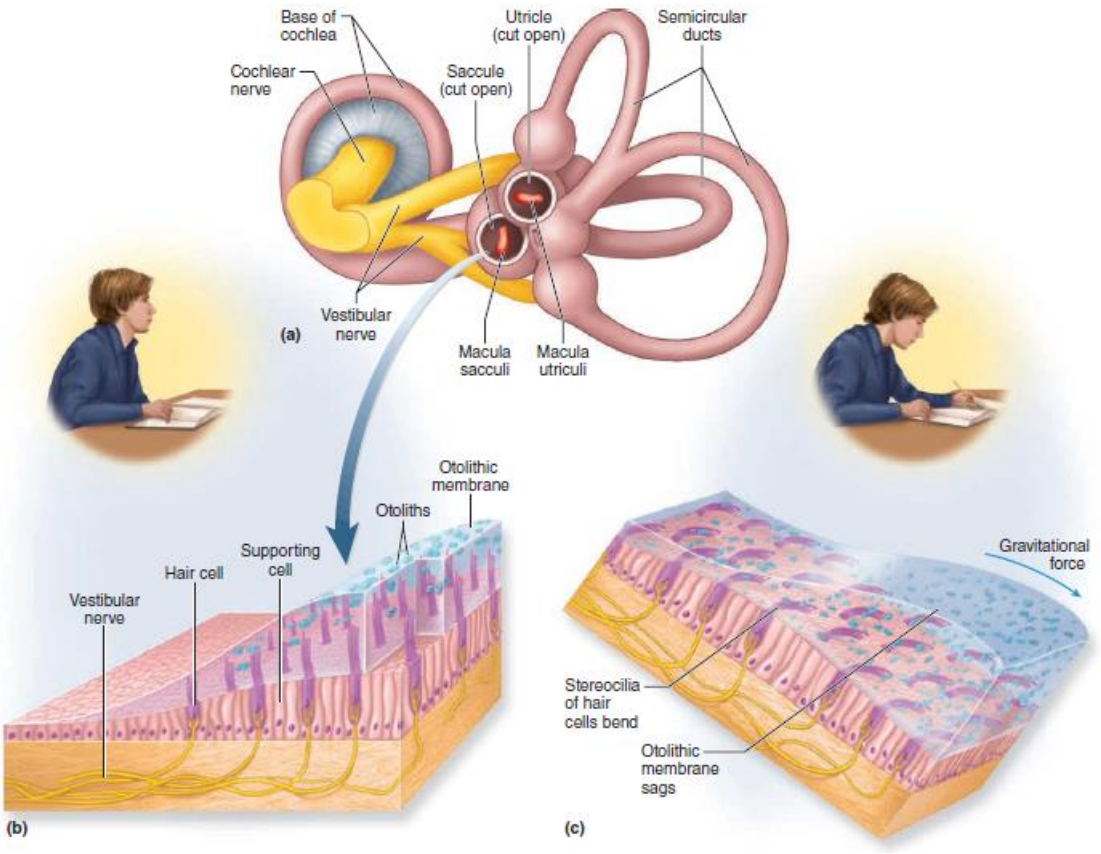

Figure 7. The Saccule and Utricle. (a) Locations of the macula sacculi and macula utriculi. (b) Structure of a macula. (c) Action of the otolithic membrane on the hair cells when the head is tilted. Human Anatomy. Kenneth S. Saladin, 2017.

The *macula utriculi* detects tilt of the head. When the head is in erect position, the otolithic membrane bears directly down on the hair cells and stimulation is minimal. When the head is tilted, however, the heavy otolithic membrane sags and bends the *stereocilia*, stimulating the hair cells.

The macula sacculi works similarly except that it is more responsive to up-and-down movements of the body (Kenneth S. Saladin, 2017).

Within each macula the hair cells are oriented with respect to an imaginary line called the striola, in the middle of the surface. The direction of hair cells polarization (arrows in the fig.8) on each side of the sriola reflects the direction in which a movement causes depolarization. (Functional Neuroscience Oswald S. 2000). At the level of the utricular striola, the hair cells have short *stereocilia* and are oriented with their polarization towards the striola. The opposite is true for the saccular striola where the hair cells have long *stereocilia* and are oriented with their polarization direction away from the striola (Fig.8) (Kingma H and Van den Berg R, 2016).

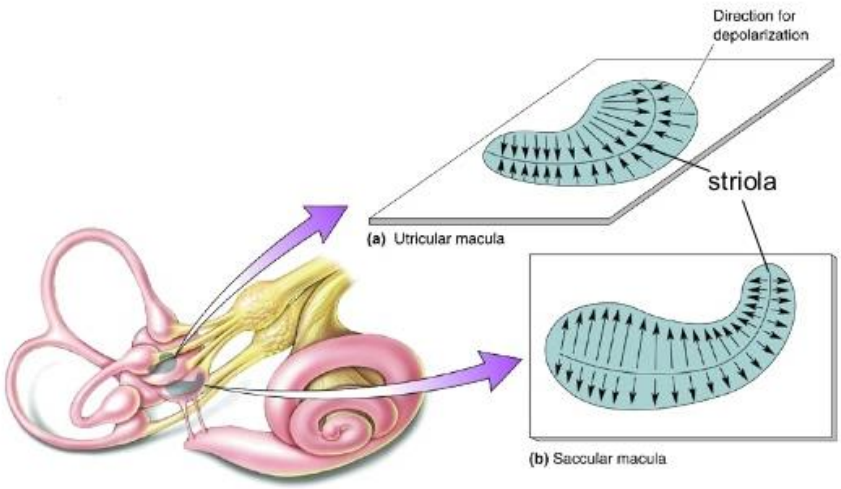

Figure 8. Position of the saccular and utricular macules. The arrows on the macules surface indicate the direction of the hair cell depolarization of each side of the striola. (https://images.app.goo.gl/NigBU7V5LisBxNcW8).

Vestibular Projection

Hair cells of the vestibular apparatus (*macula sacculi, macula utriculi*, and *crista*) synapse at their bases with sensory neurons of the vestibular nerve. The fibers of the vestibular nerve lead to a complex of four vestibular nuclei (the major integrating cores for equilibrium) on each side of the *pons* and *medulla*.

Nuclei on the right and left sides of the brainstem communicate extensively with each other, so each receives input from both the right and left ears.

The vestibular nuclei process signals about the position and movement of the body and relay information to five targets (Fig.9):

- Cerebellum: which checks head movements, eyes movements, muscle tone, and posture.
- Nuclei of the oculomotor (III), trochlear (IV), and abducens (VI) nerves: which control coupled movements of the eyes with those of the head to help maintain focus on the visual field.
- The reticular formation: which is thought to adjust breathing and blood circulation to changes in posture.
- Vestibulospinal tract: which conveys impulses down the spinal cord to maintain muscle tone in skeletal muscles to help maintain equilibrium.

- Ventral posterior nucleus in the thalamus which relays signals to the parietal lobe of the cerebral cortex. This part of the primary somatosensory area provides for the conscious awareness of the position and movements of the head and limbs. (Kenneth S. Saladin, 2017; Gerard J. Tortora and Mark T. Nielsen, 2017).

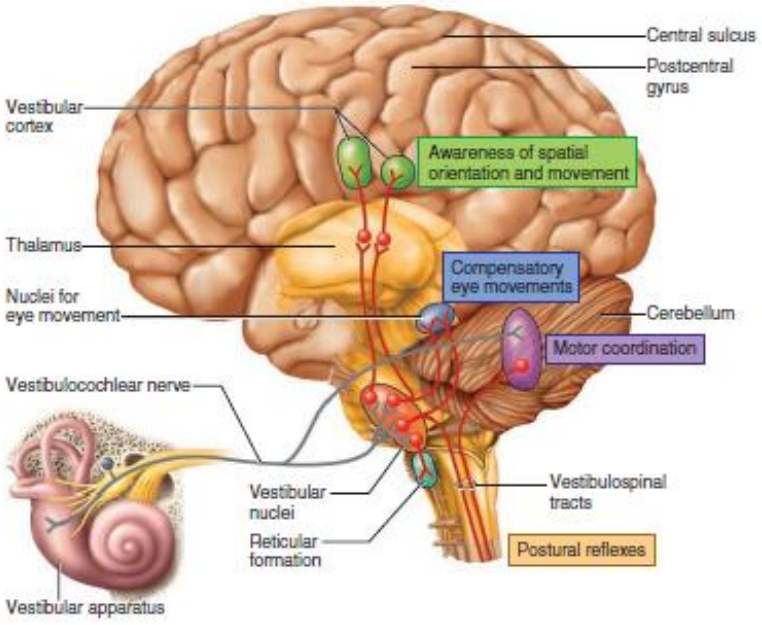

Figure 9. Vestibular Projection Pathways in the Brain. Human Anatomy. Kenneth S. Saladin, 2017.

Hair cells

Hair cells are the sensory receptors of the auditory-vestibular system in all vertebrates. Mammalian hair cells detect mechanical displacements with unparalleled temporal precision from frequencies of less than 1 Hz in the vestibular system up to about 180 kHz in the auditory system. So, they transduce acoustic stimuli, gravitational forces, and head movements into electrical signals that are relayed to higher regions in the brain to construct a three-dimensional representation of our position within the auditory and spatial landscape.

The name of these cells derives from the highly specialized hair-like elements, called hair bundle, protruding from the top of each cell.

Usually, a mature stereocilium is composed by around 2000 actin filaments (Revenu et al., 2004; Schneider et al., 2002) and it is continuously remodelled by the addition of actin monomers to the stereocilium tip, in fact the entire core of each stereocilium is renewed every 48 hours (Schneider et al. 2002). Before elongating to reach the mature levels, actin filaments into the basal region of the *stereocilia* extend down, forming a root, into the cuticular plate.

The cuticular plate is a horizontal network of actin filaments, which also contains myosin, α-actinin, fimbrin, tropomyosin, fodrin and calcium-binding proteins (Pack and Slepecky, 1995; DeRosier and Tilney, 1989).

The number of *stereocilia* changes depending on the inner ear organ, however, the diameter of cochlear and vestibular hair cell *stereocilia* is about 0.1-0.2 μm. Also, the length of the *stereocilia* varies through the different organs, but it is remarkable that vestibular hair cell *stereocilia* can be as much as 40 μm.

Kinocilium and *stereocilia*, in the single hair bundle, move as a single unit (Goodyear et al., 2005) because the structure of the hair bundle is stabilized through several different connections between individual *stereocilia* and *kinocilium*.

The precise distribution of these connections varies between hair cells of different types, but there are two main categories, tip links and lateral links, which vary during the different stages of the development (Goodyear et al., 2005; Hackney and Furness, 2013) (Fig.10).

The lateral links are horizontal filaments, which connect the rows of *stereocilia*, either along a row either between rows. In the mouse, they are classified corresponding to their localization along the *stereocilia* in ankle links (inferior connectors), shaft links (medial connectors) and top links (apical connectors).

In addition, hair cells have specialized tip links (Kachar B et al., 2000) that are 150–180 nm in length (Furness et al., 2008). Tip links connect the tip of each shorter *stereocilia* with the

neighbouring taller *stereocilia* such that they are aligned along the bundle's axis of mechano-sensitivity. Near the insertion of the links on the tips of the shorter *stereocilia* are placed the MET channels. Cadherin 23 (CDH23) and protocadherin 15 (PCDH15) have been identified as the crucial components of tip links (Beurg et al., 2009; Söllner et al., 2004; Ahmed et al., 2006). These proteins interact through their N-terminus in a Ca^{2+}-dependent manner and the concentration of Ca^{2+} affect the tension of tip-links (Fig.10).

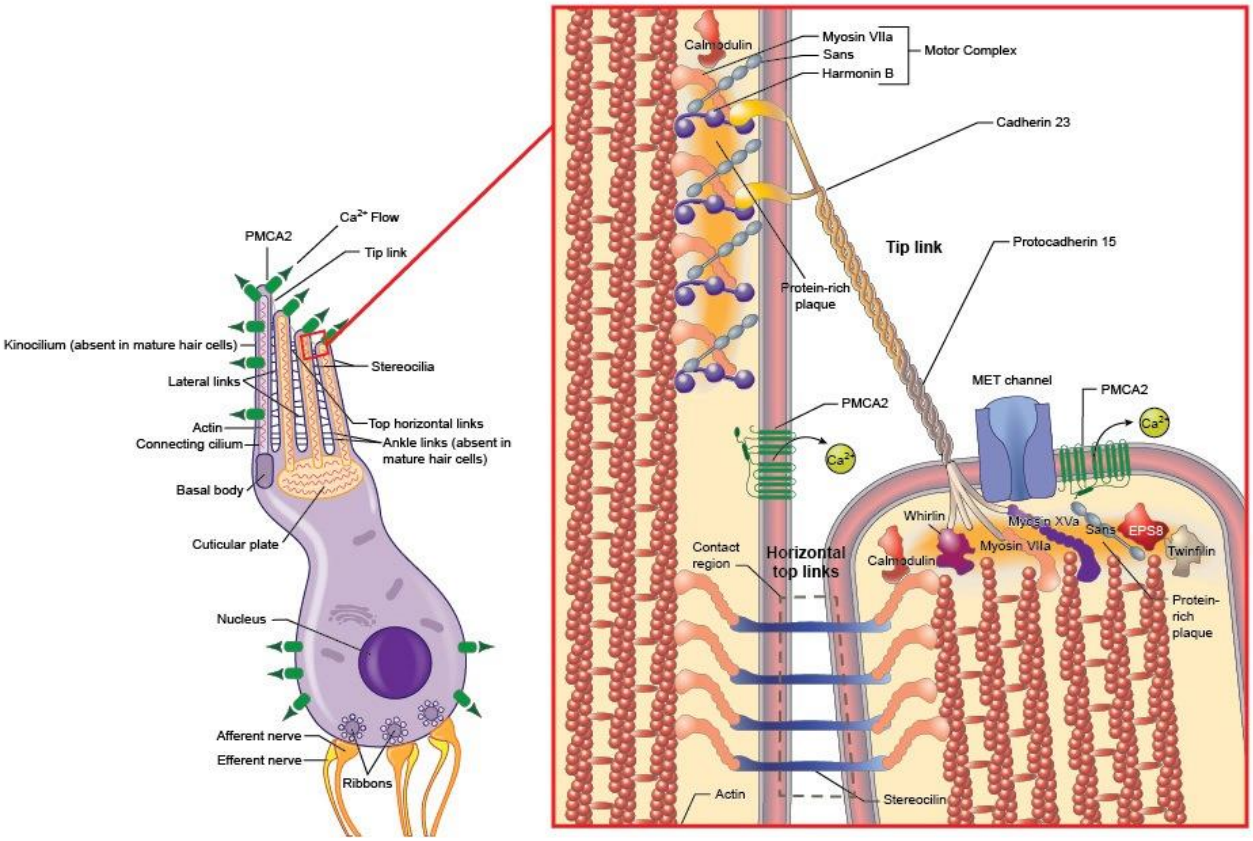

Figure 10. Structure of tip-links. The inner hair cells' hair bundle is composed of numerous stereocilia that have a core of parallel actin filaments anchored in the cuticular plate. Lateral to the tallest stereocilium is the kinocilium, which is formed from the basal body. The inset shows the molecular components of the cross-link complexes of the inner ear hair cell. In the tip-link, cadherin23 interacts with protocadherin15, harmonin, Myo7a, Myo1c, calmodulin, and Sans to help maintain the structure and function of the inner ear hair cell.
(https://mutagenetix.utsouthwestern.edu/phenotypic/phenotypic_rec.cfm?pk=1299).

Cochlear hair cells

In mammals, auditory hair cells are located along the Organ of Corti of the cochlea and transduce acoustic stimuli into an electrical response, that is relayed to the brain, enabling to perceive sound. The organ of Corti comprises three rows of OHCs and, a single row of IHCs. IHCs are supported and enclosed by additional supporting cells called inner phalangeal cells, while OHCs are mainly supported by the Deiter's cells (Marcotti and Masetto, 2010). The IHCs are located towards the center of the cochlear spiral and are described as being 'medial'. In contrast, the OHCs are on the outer periphery of the cochlear spiral, away from the center, and are hence described as 'lateral' (Fig.11).

The IHCs are the primary sensory receptor cells, and they relay sound information to spiral ganglion afferent neurons via the release of glutamate from vesicles tethered to pre-synaptic ribbons. By contrast, the role of OHCs is to enhance the sensitivity and the frequency tuning within the cochlear partition (Dallos, 1992).

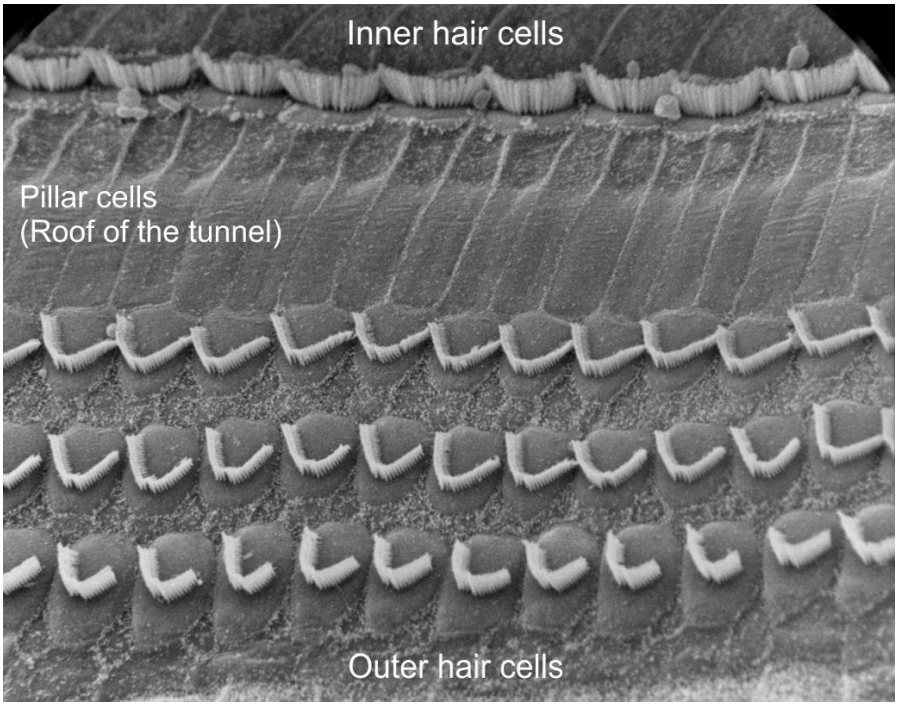

Figure 11. Surface view of mid-turn of the cochlea. One row of IHCs and three rows of OHCs are visible, along with the supporting cells that are positioned between the sensory cells. (https://lab.research.sickkids.ca/harrison/).

In cochlear hair cells, *stereocilia* are graded in height and are arranged in multiple, tightly packed rows, with the shorter rows positioned closer to the center of the apical surface. The *stereocilia* form a bilaterally symmetrical V-shaped descending staircase (Fig.11).

Cochlear hair cells have tonotopic organization. It means that cochlear hair cells are positioned, along the cochlear sensory epithelium, according to their best response frequency. In fact, high frequency cells are located at the base, whereas low-frequency cells are located at the apex.
Moreover, the morphological properties of hair cells change progressively along the cochlea, indeed the longest hair bundles are located at the apex in the low-frequency cells and the shortest are at the base in the high-frequency cells (Fettiplace and Hackney, 2006).
Hair cell differentiation progresses in a basal to apical direction for several more days and it is completed around postnatal day 20 (P20), around 8 days after the onset of hearing in rodent (P12); Marcotti and Masetto, 2010). Several distinct patterns of spontaneous, experience-independent Ca^{2+} activity across the auditory sensory epithelium orchestrate the differential maturation of OHCs and IHCs (Johnson et al, 2013) to shape the final stages of auditory organ development.
Adult IHCs are innervated by 5–30 type I afferent fibers that form small contacts or boutons, (Liberman et al., 1990). The number of boutons depends on the position of the cell along the cochlea, with basal, high frequency cells having more endings than their apical, low frequency counterparts.
The afferent fibers contacting each IHC have different thresholds, firing rates, and operating ranges (Liberman, 1982), governed, at least in part, by the release of glutamate from IHC ribbon synapses (Grant et al., 2010) and differences in the properties of individual presynaptic active zones within single IHCs (Frank et al., 2009).
The firing activity in the immature afferent fibers is driven by excitatory postsynaptic currents (EPSCs) triggered by the release of glutamate from spontaneously active immature IHCs (Glowatzki and Fuchs, 2002). This activity propagates to higher centers of the auditory brainstem as irregular rhythmic patterns that are organized in bursts (Kandler et al., 2009; Tritsch et al., 2010).
When IHCs stop firing action potentials at the onset of hearing, the firing pattern of the spiral ganglion neurons (SGNs) takes on the mature characteristic of continuous, non-bursting, spontaneous spiking that is modulated by IHC synaptic vesicle release.
In addition to afferent activity, another level of control in adults comes from efferent neurons that project from the lateral olivary complex (LOC) and form axodendritic synapses with the afferent terminals innervating IHCs.
This input allows the brain to influence the development both of hair cells and of the auditory pathway directly.

Vestibular hair cells

Vestibular sensory epithelia of Amniotes contain two Types of sensory cells, called Type I and Type II hair cells (HCs). Type I hair cells are present in reptiles, birds, and mammals, but not in fish or amphibians (Wersall and Bagger-Sjoback 1974; Lysakowski 1996). In mammals, both type I and type II hair cells are found along the whole *cristae* and *maculae*. In reptiles and birds, the same is true for type II hair cells, but type I hair cells have a more restricted distribution to the central zones of the *cristae* and the striola of the utricular macula (Rosenhall 1970; Jorgensen and Anderson 1973; Jorgensen 1974, 1975; Brichta and Peterson, 1994; Lysakowski, 1996).

During embryonic stages of development all vestibular hair cells express an Na^+ current (I_{Na}), an inward rectifying K^+ current (I_{K1}), and a conventional delayed rectifying K^+ current ($I_{K,v}$), (they will be described later) (Eatock and Hurley, 2003; Géléoc et al., 2004; Wooltorton et al., 2007). Although the Ca^{2+} current has not yet been investigated in rodent embryos, its expression is likely to be consistent with data in chick embryo hair cells (Masetto et al., 2000) and to coincide with the presence of afferent nerve contacts.

Studies suggested that vestibular hair cells in early post-natal rats express neuronal-like tetrodotoxin (TTX)-sensitive Na^+ channels able to generate Na^+-driven action potentials and to induce activity-dependent brain-derived neurotrophic factor (BDNF) secretion. The activation of Na^+ channels may be of functional importance during the vestibular system maturation and differentiation. However, during the maturation of the vestibular system, I_{Na} disappears during the second post-natal week and electrical stimulation fails to induce BDNF release (Chabbert et al., 2003).

The afferent fibers in amniotes are classified into three groups: calyx fibers, which envelop type I hair cells; bouton afferents that form synaptic contacts exclusively with type II hair cells; and dimorphic fibers, which have both calyceal endings innervating type I hair cells as well as bouton endings contacting type II hair cells. These afferent fibers have different distributions along the sensory epithelia. In mammalian cristae, calyx units are confined primarily to a central zone, bouton units predominate in the peripheral zone and dimorphic units are located throughout the epithelium. (Lysakowski and Goldberg, 2004).

In both Type I and type II hair cells, the afferent neurotransmitter is glutamate that binds to the postsynaptic AMPA (Alpha-amino-3-hydroxy-5-methyl-4-isoxazolepropionate) receptors on

the afferent nerve terminal (Glowatzki et al., 2008). Concerning efferent innervation, fibres directly contact type II hair cells or type I calyx; however, their role is not well understood.
While the efferent neurotransmitter is the acetylcholine, which is principally responsible for the inhibitory and excitatory responses and it can bind to metabotropic or ionotropic cholinergic receptors located in the type II hair cell's basolateral membrane or in the calyx, where it increases the background afferent discharge and reduces the sensitivity or gain of afferents to vestibular stimulation (Poppi et al., 2018).
In the sensory epithelium between Type I and type II hair cells, there are supporting cells which are bipolar cells, characterized by the presence of short microvilli and large secretory granules in the apical region and by the nucleus in the basal region. The supporting cells, like the vestibular hair cells, differ in number according to the organ considered. They are around 1858 ± 220 in each mouse crista, 2073 ± 18 in saccular macula and 2754 ± 50 in utricular macula (Desai et al., 2005a; Desai et al., 2005b). It has been hypothesized that the supporting cells are involved in several important functions, such as mediators of development, death, and phagocytosis of the hair cells (Bird et al., 2010; Monzack and Cunningham, 2013). Moreover, supporting hair cells could be crucial for the synthesis and maintenance of the cupula and to mediate glutamate clearance at synapses in order to prevent excitotoxicity (Pujol and Peul, 1999; Gale and Jagger, 2010).
Finally, supporting cells are involved in removing damaged or dead hair cells from the sensory epithelium (Monzack and Cunningham, 2013).

Ribbon Synapse

Ribbons are electron-dense organelles that tether many synaptic vesicles (SV) close to the synaptic vesicle release sites (Safieddine et al., 2012), probably to facilitate high rates of sustained synaptic transmission and coordinated, synchronous release of multiple vesicles (Glowatzki and Fuchs, 2002; Goutman and Glowatzki, 2007; Grant et al., 2010). The ribbon synapse is unique to sensory systems that have to encode sustained and graded stimuli (Matthews and Fuchs, 2010).

In hair cells, synaptic ribbons, can be spherical, planar, or oblong in shape and variable in size, tethering from 20–400 vesicles. Even within one hair cell, individual ribbons can vary in size and shape. Although these organelles in non-mammalian hair cells can be somewhat larger (200–400 nm in diameter), ribbons in mammalian hair cells are ≤200 nm width. (Matthews et al., 2010 review).

How ribbons might coordinate the fusion of independent vesicles remains mysterious, but in the auditory system, such synchronization is likely a major functional role of ribbons, because it promotes the precisely timed activation of afferent neurons that is required for encoding speech patterns and for sound localization (Matthews et al., 2010)

Vesicles tethered to the bases of ribbons and adjacent to the presynaptic membrane form the Readily Releasable Pool (RRP), which gradually increases to 600–800 vesicles per IHC by about P6 (Johnson et al., 2005; Khimich et al., 2005).

Various lines of evidence indicate that either $Ca_v1.3$ or $Ca_v1.4$ L-type calcium channels drive release at ribbon synapses, depending on cell type.

The biophysical properties of the synaptic machinery change during development to convey the different types of information encoded by immature and adult cells. Immature, spiking IHCs release neurotransmitter with a high Ca^{2+} cooperativity (Johnson et al., 2005; Johnson et al., 2009), which allows better synchronization of neurotransmitter release with the action potentials. By contrast, mature IHCs respond to sound stimulation with small, graded receptor potentials, and exocytosis is linearly dependent on Ca^{2+} influx (Johnson et al., 2005; Brandt et al., 2005).

Neurotransmitter release requires the calcium sensor otoferlin, a protein involved in the control of the exocytosis process. However, some studies demonstrate the presence of spontaneous postsynaptic firing activity at the afferent calyx endings of vestibular hair cells from $Otof^{-/-}$ mice. This could mean that otoferlin is not essential for the associated hair cell synaptic vesicle priming or fusion. In addition, residual evoked vestibular potentials and Ca^2-dependent

exocytosis were observed in Otof$^{-/-}$ hair cells, indicating that, if otoferlin is a Ca^2-sensor, another one is present in these vestibular mutant hair cells (Dulon et al., 2009).

Mechano-electric transduction

Mechanical deflection of the hair bundle (Fig.12), normally induced by physiological stimuli, increases the open probability of MET channels located at the tip of *stereocilia*. The resulting depolarizing inward current generates a receptor potential. The information encoded in this electrical response is transmitted to the auditory or vestibular afferent nerve fibres via the $Ca2^{+}$-induced release of neurotransmitter from the hair cell's basal pole. In this way sensory information is relayed to the brain enabling us to perceive sound and maintain balance (Marcotti and Masetto 2010).

The molecular identity of the channel involved into mechano-electrical transduction has been largely investigated (Fettiplace and Hackney, 2006; Furness and Hackney, 2006) but is still unclear.

As mentioned before, mature tip links are formed by PCD15 and CDH23 molecules (Fig.10). There is evidence that, at the lower end of the tip link, PCD15 could be connected to transmembrane channel-like protein 1 and 2 (respectively, TMC1 and TMC2), which contribute to the subunits forming the MET channel (Maeda R et al., 2014).

Moreover, some of these proteins could have Ca^{2+}-binding sites to account for the multiple Ca^{2+} effects on the MET current, but the molecular identity of these components is still unknown (Giese APJ et al., 2017).

Cilia movement toward the *kinocilium* (excitatory deflection) increases tip-link tension, which is then transmitted to the MET channels resulting in their opening (Marcotti and Masetto, 2010). MET opening causes the flow of K^{+} (but also $Ca2^{+}$) from the endolymph into the hair cell and the resultant depolarization. Thus, voltage-gated channels open and Ca^{2+} enter the cell leading to glutamate calcium-dependent exocytosis onto the afferent nerve terminal (Fig.12).

A characteristic of the transducer currents is that it can adapt. This phenomenon acts as negative feedback, resetting the operating range and sensitivity of the MET channel. Although the exact mechanism underlying Ca^{2+}-induced adaptation (i.e., channel closure) is not known, it has different time-dependent components (Eatock, 2000; Fettiplace, 2009). The fastest component of adaptation, less than a millisecond in mammals, is thought to be caused by Ca^{2+} that block the transducer channel itself (Fettiplace R and Kim KX, 2014).

Whereas the slower components, which takes few tens of millisecond, involves a change in the attachment point of the element connected to the MET channels. During the excitatory deflection, the increased tension in the tip link causes its upper attachment point to slip down the side of the stereocilium. It results in a reduction of the tension in the elastic element and

adaptation. At the end of the stimulus, the tension is reduced, and the attachment point of the tip link is pulled back up the stereocilium by a motor ascending along the actin backbone of the stereocilium to re-tension the tip link (Fettiplace, 2017). In non-mammals the motor is the myosin IC (Gillespie and Cyr, 2004), whereas in mammals it could be the myosin VIIa (Kros et al., 2002) or myosin VI (Marcotti W et al., 2016) (Fig.10 inset).

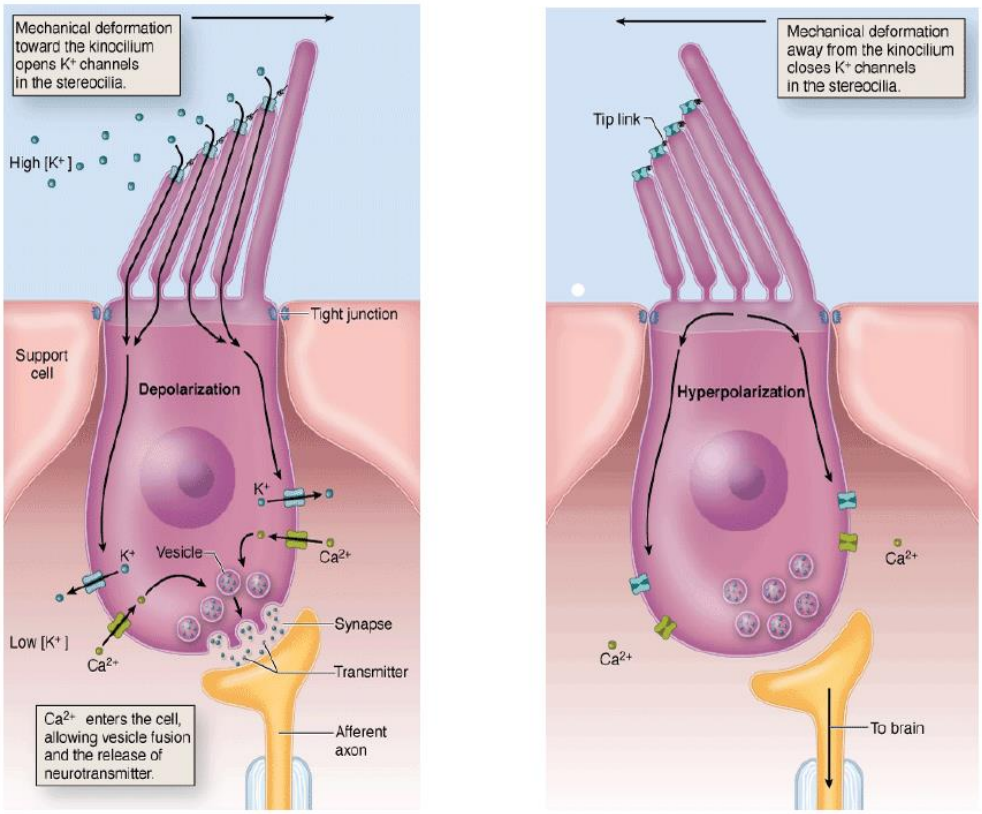

Figure 12. Schematic diagram of mechanotransduction in hair cells.
On the left is shown the consequence of an excitatory deflection, whereas on the right is shown the consequence of an inhibitory deflection. In particular, deflection toward the kinocilium (left) results in the opening of MET channels, which carry a depolarizing transducer current. Depolarization carries to the opening of K^+ and Ca^{2+} channels in the basolateral membrane with the consequent receptor potentials, depolarization and the release of vesicles containing the neurotransmitter (glutamate). Glutamate diffuses in the synaptic cleft and binds with AMPA receptors at the post-synaptic (afferent) element, depolarizing it. Depolarization is converted to action potentials. Otherwise, deflection toward the smallest stereocilium results in the closing of all MET channels. Mescher, 2011.

Voltage-dependent K^+ channels in Cochlear hair cells

Immediately after terminal mitosis, IHCs and OHCs begin to express an inward rectifier (I_{K1}) K^+ currents and a small outward delayed rectifier (I_K) current (Marcotti et al., 2003 Pt 2).

I_{K1} is an inward rectifier K^+ current, which has a very fast kinetics, is K^+-selective, and is blocked by Ba^{2+}. gK1 increases in size until the onset of hearing after which it rapidly decreases to a small current (Marcotti et al.,1999).

After birth, I_K develops in a 4-AP insensitive outward K^+ current that causes repolarization, known as $I_{K,neo}$ (Marcotti and Kros, 1999). The depolarized activation range of the outward current and the small size of the inward rectifier I_{K1} make the 'resting potential' relatively more positive.

In OHCs, the array of ion channels remains unchanged from birth up to the onset of functional maturation at P8, whereupon I_K is down-regulated and the negatively activating K^+ current characteristic of adult cells, $I_{K,n}$, begins to be expressed (Marcotti and Kros, 1999). $I_{K,n}$, which is carried by KCNQ4 channels, is crucial for maintaining the OHCs' resting membrane potential.

The functional maturation of OHCs from around P8 coincides with the appearance of the cells' electromotile activity (He et al., 1994; Marcotti and Kros, 1999), the expression of the apamin-sensitive small conductance Ca^{2+}activated K^+ current ISK2 (Oliver et al., 2000), and innervation by cholinergic efferent fibers originating from the superior olivary complex (Shnerson et al., 1981). From birth up to about P10–P12, all K^+ currents (I_K, I_{K1}, and ISK2) in OHCs continue to increase in amplitude (Marcotti et al., 1999; 2003 Pt 2; 2004), from this moment on I_{K1} and ISK2 disappear.

As regards IHCs, the acquisition of the BK-current $I_{K,f}$ and the delayed rectifier K^+ current $I_{K,n}$ (Marcotti et al., 2003 Pt 2) around P12 represents their first sign of functional maturation. Moreover, three additional K^+ currents are present in mature IHCs: the delayed rectifier $I_{K,s}$, (Marcotti et al., 2003 Pt 2), and an additional BK-type current named $I_{K(Ca)}$ (Marcotti et al., 2004 Pt 2).

$I_{K,f}$ is a large current (about 10 nA at 0 mV) that shows rapid activation kinetics. Moreover, it activates around -85 mV, and it is directly modulated by the voltage-dependent release of Ca^{2+} from intracellular Ca^{2+} stores (Marcotti et al., 2004 Pt 2).

$I_{K,n}$ was originally described in OHCs (Housley and Ashmore, 1992), and it is expressed differently in the mouse cochlea. Indeed, its size in IHCs is about 45% of that in the OHCs.

In IHCs, SK2 channels may contribute to the repetitive action potential waveform in immature IHCs (Marcotti et al., 2004 Pt 3; Johnson et al., 2007).

The efferent contacts on IHCs are mainly eliminated from around the onset of hearing (Simmons et al., 1996), which is immediately followed by the down-regulation of SK2 channels (Glowatzki and Fuchs, 2000).

Voltage-dependent K^+ channel in Vestibular hair cells

Type I and type II hair cells express different arrays of voltage dependent ionic channels, that attribute specific electrophysiological properties to the two vestibular cell types.

Vestibular hair cells of mouse maturate earlier than cochlear hair cells, around postnatal day (P4).

A small outwardly rectifying delayed rectifier K^+ current (IDR) is present in vestibular hair cells at embryonic day 14 and it increased in amplitude during the next several days (Géléoc et al., 2004).

This current, soon after birth, constituted the main current in vestibular hair cells of mouse (Géléoc et al., 2004) and it was demonstrated that it is blocked by 4-aminopyridine (4-AP) or Ba^{2+} (Meredith and Rennie, 2016).

As far as inward rectifying current is concerned, I_{K1}, is always evident in mature type II and sometimes in Type I hair cells. (Meredith and Rennie, 2016). This current is mediated by Kir2.1 channels and are blocked by external Cs^+ and Ba^{2+}. Current injections in type II hair cells expressing Kir2.1 channels, induce faster and smaller amplitude voltage responses. This indicates that I_{K1} can lower the time constant and extend the hair cell response to higher stimulation frequencies.

In mature vestibular type II and type I hair cells another inward rectifying K^+ current, called Ih, has been identified, which is a K^+ and Na^+ inward rectifier current activated by hyperpolarization. Ih is carried by HCN1 channels; robust expression of Ih was found in 89% of type II hair cells and 78% of type I hair cells (Horwitz GC et al., 2011).

In addition, in type II vestibular hair cells, after the maturation, appears an A-type outward potassium current ($I_{K,A}$), which activates between -60 and -50 mV, and it is characterized by a fast activating and fast inactivating current.

Concerning to Type I hair cells, from E18 in mice (Géléoc et al., 2004), and post-natally in rats (Eatock and Rüsch, 1997), the biophysics and voltage responses of these cells begin to diverge due to the acquisition of a negatively activating K^+ current $I_{K,L,}$ which activates at about –100 mV, is fully active at –60 mV and does not inactivate.

The high expression density of KL channels means that type I cells have a larger current active around their resting membrane potential compared to type II cells (Rüsch and Eatock, 1996). In consequence, type I cells have low input resistances (10–100 MΩ) far below those of type II cells (>300 MΩ), which makes their activation kinetics much faster but their response amplitudes smaller. $I_{K,L}$ resembles $I_{K,n}$, which is carried by KCNQ4 in cochlear hair cells

(Marcotti and Kros, 1999). However, the kinetic and pharmacological properties of $I_{K,L}$ differ between immature and adult type I hair cells and may be carried by two different channels: KCNQ4 during immature stages and ether-a-go-gorelated (erg) in adults (Hurley et al., 2006). The presence of $I_{K,L}$, together with the concomitant maturation of the calyx (Goldberg, 1991; Songer and Eatock, 2013), is likely to supply fast, linear representations of head motion to reflex pathways.

These channels are highly permeable to K^+ and significantly permeable to Cs^+. Pharmacologically they are blocked by internal TEA, and by micromolar concentrations of external 4-AP and Ba^{2+} (Li et al., 2010).

It has been shown that K^+ exiting through $G_{K,L}$ can produce a significant shift of the K^+ current reversal potential ($\Delta V_{rev}K^+$), which has been attributed to K^+ accumulation in the residual calyceal synaptic cleft, between the calyx inner membrane and the basolateral membrane of the type I cell (Lim et al., 2011; Contini et al., 2012; Contini et al., 2017). This substantial shift of $VrevK^+$ was found either in situ or in dissociated Type I hair cells, consistent with the calyx inner membrane being tenaciously attached to the hair cell basolateral membrane (Spaiardi et al., 2020a).

$I_{K,Ca}$ is a minor contributor to the macroscopic K^+ conductance of the vestibular Type I HC. In fact, in a minority of cells may be present a small conductance calcium-activated K^+ current (SK) and a large conductance calcium-activated K^+ current (BK) components (Rennie and Correia, 1994).

Voltage-dependent Ca^{2+} channel in Cochlear hair cells

Mouse embryo IHCs express a Ca^{2+} current (ICa), carried almost exclusively by $Ca_v1.3$ Ca^{2+}, a class of voltage-gated L-type Ca^{2+} channels (LTCCs) (Platzer et al., 2000; Brandt et al., 2003; Michna et al., 2003; Beurg et al., 2010). In late embryonic IHCs, these channels promote membrane capacitance changes, which are indicative of synaptic vesicle fusion at the presynaptic cell membrane, (Marcotti et al., 2003 Pt 3; Johnson et al., 2005).

In neonatal OHCs, Ca^{2+} channels seem to play a role in maturation, since OHCs from $Ca_v1.3$-deficient ($Ca_v1.3^{-/-}$) mice degenerate shortly after the onset of hearing.

Ca_v channels are macromolecular complexes comprising several subunits. The Ca^{2+} selective channel pore is formed by 1 of 10 α1-subunit isoforms, and accessory subunits include 1 of 4 different β-subunit isoforms and 1 of 4 different α2δ subunits (Buraei Z et al., 2010; Dolphin AC 2012). The $\alpha_1$subunit determines most of the channel's biophysical and pharmacological properties; accessory subunits modify these properties and in addition influence the abundance and localization of Cav channels.

Ca_v1 family is composed by four members: $Ca_v1.1$, $Ca_v1.2$, $Ca_v1.3$, and $Ca_v1.4$. Both $Ca_v1.3$ and $Ca_v1.4$ channels activate at relatively hyperpolarized potentials, and they inactivate slowly (Baumann et al., 2004; Koschak A et al., 2001).

$Ca_v1.3$ Ca^{2+}channels are expressed most abundantly in IHCs and OHCs and in VHCs.

Alternative splicing is a key regulator for the functional properties of Cav1 channels, and the best understood is about the COOH terminus in the $Ca_v1.3$α1 channel. This COOH is part of a domain called COOH-terminal modulatory domain (CTM) and competes with calmodulin (CaM) in binding the IQ-domain of the channels, this way weakens CaM-mediated Ca^{2+}-dependent inactivation. Also, the CTM can change the normal physiology response of the channels (Bock et al., 2011).

L-type Ca^{2+} channels are arranged in clusters, and can form a "nanodomain", that control exocytosis. Ca^{2+} nanodomain is a term used when the distance between a Ca_V channel and a vesicular fusion sensor is less than 100 nm and when only a single channel open is required to generates a Ca^{2+} increase sufficient to activate the vesicular sensor (Pangrsic et al., 2018).

L-type Ca^{2+} channels show a high sensitivity to dihydropyridine (DHP) Ca^{2+} channel modulators. Their Ca^{2+}-selective pore is formed by different DHP-sensitive α1 subunit isoforms (α1S, α1C, α1D, α1F). In IHCs, L-type Ca^{2+} channels formed by a1D subunits (D-LTCCs) possess biophysical and pharmacological properties distinct from those of a1C containing C-LTCCs.

Studies provided evidence that most of the biophysical differences are determined by a1D. The presence of a1D subunit leads to more negative range of current activation and slower current inactivation during depolarizations, allowing these channels to mediate long lasting Ca^{2+} influx during weak depolarizations (Koshak et al, 2001). Such properties allow LTCCs to control tonic neurotransmitter release in hair cells (Kollmar R et al., 1997; Moser T and Beutner D 2000).
In addition, it has also been described for the first, that DHP inhibition of a1D is voltage-dependent and favored at more positive voltages (Koshak et al.,2001).

Voltage-dependent Ca^{2+}channel in Vestibular hair cells

Type I and type II hair cells express similar voltage-gated Ca^{2+} channels, that have a rapid activation kinetics and a negligible inactivation.

Chicken embryo semicircular canal type I and type II hair cells express a similar voltage-dependent L-type ICa, whose main features are: activation above -60 mV, fast activation kinetics, and scarce inactivation (Masetto et al., 2005).

ICa is already active at rest in the most peripheral region of the chicken embryo *cristae* (Zone 1) type II hair cells, whose resting membrane potential was on average slightly less negative than -60 mV. Conversely, ICa is closed at rest in type II hair cells from Zone 2 (the intermediate region between Zone 1 and 3) and Zone 3, at the center of the *cristae* nor in type I hair cells since their resting membrane potential is significantly more negative than -60 mV. (Masetto et al., 2005).

In rat type II hair cells of *cristae* following large depolarization, ICa decay with time constants of several hundred milliseconds.

In rat type I hair cells, the voltage-dependence of the ICa activation curve is slightly leftward shifted of few millivolts compared to type II. The reason of this difference is not clear, this may be due to the different subunit composition of Ca^{2+} channels. (Bao et al., 2003).

Type I and type II hair cells show the same average ICa amplitude values between -70 mV and -40 mV, while at more depolarized potentials the average current of type II cells is larger than Type I cells. No functional significance about this difference is known (Bao et al., 2003).

The majority of the Ca^{2+} channels in vestibular hair cells express the $Ca_v1.3a1D$ subunits of the L-type Ca^{2+} channels.

As in the cochlear hair cells, a major portion of whole-cell Ca^{2+} currents in vestibular hair cells are deriven from the a1D dihyropyridine-sensitive Ca^{2+} channels (Kollmar et al. 1997a; Zidanic and Fuchs 1995).

Glutamate exocytosis in cochlear and vestibular hair cells

The timely and reliable processing of auditory and vestibular information within the inner ear requires sophisticated sensory transduction pathways.

On a cellular level, these demands are met by hair cells, which respond to sound waves or alterations in body positioning by releasing glutamate filled synaptic vesicles (SVs) from their presynaptic active zones (AZ) with unprecedented speed and temporal fidelity, thereby initiating the auditory and vestibular pathways (Pangrsic. T et al., 2018).

Precisely, after the excitatory deflection of the hair bundle, due to depolarization, it occurs the opening of voltage-dependent calcium (Ca_V), allowing Ca^{2+} entry, which stimulates the fusion of synaptic vesicles to the cell membrane (Fig.12).

The synaptic vesicles fuse with the presynaptic element and release the excitatory neurotransmitter, glutamate, into the synaptic cleft (Glowatzki et al., 2008).

Generally, ribbons (mentioned before), are considered to provide molecular scaffolding at the AZ, tether a large complement of SVs and, hence, are thought to facilitate continuous vesicular replenishment to the release site. Moreover, ribbons are important for clustering presynaptic Ca^{2+} channels (Frank. T et al., 2010; Jean. P et al., 2018) and may act as physical Ca^{2+} diffusion barriers to produce spatially tightly confined Ca^{2+} hotspots (Graydon. CW et al., 2011).

Packing 3,000 glutamate molecules into a 37-nm diameter SV would yield an intravesicular concentration of ~200 mM glutamate.

The excitatory neurotransmitter opens the glutamate-receptor (GluR) channels in the post-synaptic element, so the resultant excitatory postsynaptic current (EPSC) evoked, depolarize post-synaptic membrane, activating voltage-gated Na^+ (NaV) channels in the afferent fiber, which generate action potentials (spikes). Then, spikes propagate down the myelinated afferent process, through the bipolar cell body located in the ganglion, and along the central afferent process toward secondary neurons in the brain stem and the cerebellum (Eatock and Songer, 2011).

Finally, while neurons mainly employ P/Q- and N-type CaV2.1 and 2.2 Ca^{2+}-channels for Ca^{2+}-influx–secretion coupling (Catterall. WA and Few. AP 2008), IHC AZs utilize L-type $Ca_v1.3$ Ca^{2+} channels for this purpose (Platzer. J et al., 2000; Dou H et al., 2004). Recent work revealed that the activation kinetics and open probability of L-type $Ca_v1.3$ Ca^{2+} channels, not only differ based on their tonotopic position along the cochlear axis (Zampini. V et al., 2014; Meyer. AC 2009), but also depend on their subcellular AZ localization (Frank. T et al., 2009), thereby suggesting the location-dependent presence of yet-to-be-identified regulatory proteins. In this

context, $Ca_v1.3$ Ca^{2+} channels show to be regulated by several modulatory proteins, including Gipc3 and CaBP2 (Ohn T-L et al., 2016; Picher. MM et al., 2017; Pangrsic. T et al., 2018).

Morphologically, AZ-tethered SVs are usually classified into two main populations, the membrane-proximal and the ribbon-associated pool of SVs. The fast, exponential component of exocytosis, which is usually recruited by brief depolarizations, is believed to represent the fusion of the readily-releasable pool of SVs (RRP) (Beutner. D et al., 2001; Johnson. SL et al., 2009). This RRP might be further subdivided into two kinetically distinct SV pools according to postsynaptic recordings of spiral ganglion neurons (SGN) excitatory postsynaptic currents (EPSCs) (Goutman. JD., 2007). While the morphological correlate of the RRP is likely represented by the membrane-proximal SVs, the sustained component of exocytosis or slowly-releasable pool of SVs may reflect continuous replenishment of ribbon-associated SVs after initial RRP depletion (Frank. Tet al., 2010; Beutner. D and Moser. T 2001; Johnson. SL et al., 2009; Pangrsic. T et al., 2010).

Mammalian IHC are not prone to coordinated multivesicular release per synapse (cMVR) during spontaneous and sustained exocytosis (Glowatzki. E and Fuchs. PA 2002), but rather may be dominated by a singol release per synapse (UVR). In essence, this may create a highly efficient synaptic transfer of 1 SV for 1 action potential (AP).

It may seem odd that a ribbon-type AZ would have so many SVs, but only utilize them one at a time. However, a 1 SV to 1 AP ratio is maximally efficient, and this will help IHCs maintain high rates of continual release by mitigating the onset of presynaptic fatigue and reduce the metabolic burden of excess glutamate recycling (Grabner P et al., 2018).

Introduction

In mammals, the primary sensory cells are the IHCs of the cochlea, and the type I and type II hair cells of the vestibular system. Acoustic stimuli or head movements cause inflow of cationic current through MET channels located at the tip of the *stereocilia*, resulting in depolarization that brings to the opening of Ca^{2+} and K^{+} channels located at basolateral membrane of the cell. Neurotransmitter release at the afferent nerve terminal is modulated by Ca^{2+} inflow to allow the synaptic vesicle fusion.

Both auditory and vestibular hair cells express voltage-gated L-type Ca^{2+} channels containing the pore-forming $Ca_v1.3$ subunit (previously known as α1D), which are characterized by a negative voltage of activation (about -60 mV) and negligible voltage-dependent inactivation (Platzer et al., 2000; Bao et al., 2003; Johnson and Marcotti, 2008; Zampini et al., 2013).

Pharmacologically, L-type ($Ca_v1.1$ to $Ca_v1.4$) Ca^{2+} channels are identified by their sensitivity to dihydropyridines (DHPs) such as nimodipine and nifedipine (antagonists), however, the $Ca_v1.3$ subunit is relatively insensitive to DHPs compared to $Ca_v1.1$, 1.2. and 1.4 subunits (Koshack et al., 2001; Xu and Lipscomb e 2001).

Previous work has indicated that ∼90% of the Ca^{2+} current in IHCs is carried by the $Ca_v1.3$ subunit (Platzer et al. 2000; Jeng et al., 2020a). So, the residual Ca^{2+} current (∼10%) could be carried by the $Ca_v1.4$ subunit (Brandt et al., 2003).

Consistent with the critical role of $Ca_v1.3$ Ca^{2+} channels in hair cell Ca^{2+} dependent exocytosis, $Ca_v1.3^{-/-}$ mice are deaf (Platzer et al., 2000; Brandt et al., 2003), but do not show vestibular deficits (Platzer et al., 2000; Dou et al., 2004).

A pharmacological study from rat semicircular canal crista hair cells has indicated that the level of expression of $Ca_v1.3$ Ca^{2+} channels is comparable to that of the cochlear IHCs (Bao et al., 2003). However, vestibular utricle hair cells from $Ca_v1.3^{-/-}$ mice appear to express a large residual Ca^{2+} current (~50%, Dou et al., 2004), which could potentially drive some signal transmission to the afferent fibres, at least during linear vertical head accelerations. Currently, it is unknown whether a substantial residual Ca^{2+} current is also expressed in $Ca_v1.3^{-/-}$ semicircular canal hair cells and whether its size is similar between type I and type II hair cells. The recently identified non-quantal signal transmission at type I hair cell synapses (Eatock, 2018; Contini et al., 2017; Contini et al., 2020), together with the eventual residual Ca^{2+} currents in vestibular hair cells from $Ca_v1.3^{-/-}$ mice, could contribute, at least in part, to the latter's milder anomalous vestibular phenotype. Non-quantal transmission, which has not been reported in auditory hair cells, involves intercellular K^{+} accumulation in the synaptic cleft occurring during

the activation of a low-voltage activated outward rectifying K^+ current $I_{K,L}$ (Lim et al, 2011; Contini et al., 2012; Contini et al., 2017; Spaiardi et al., 2017; Contini et al., 2020; Spaiardi et al., 2020a).

In this study, we have performed whole-cell patch clamp recordings from IHCs and both type I and type II hair cells from the mammalian crista of wild-type and $Ca_v1.3^{-/-}$ mice using the same experimental conditions in terms of extracellular Ca^{2+} and temperature. We have found that both IHCs and vestibular hair cells from $Ca_v1.3^{-/-}$ mice have < 20% of residual Ca^{2+} current compared to control mice. Thus, the large residual ICa^{2+}found in utricular hair cells from $Ca_v1.3^{-/-}$ mice (Dou et al., 2004), could be justified by a different expression of $Ca_v1.3$ Ca^{2+} channel in these organs; this would allow to retain some Ca^{2+}-dependent neurotransmitter exocytosis in vestibular organs.

Different from cochlear IHCs, our data confirmed that the normal maturation of K^+ conductances of both type I and type II hair cells doesn't require $Ca_v1.3$ Ca^{2+} channels. Given that $I_{K,L}$ is responsible for intercellular K^+ accumulation in the synaptic cleft of type I hair cells also in $Ca_v1.3^{-/-}$ mice, we assumed that non-quantal signal transmission might also contribute to the normal functioning of $Ca_v1.3^{-/-}$ mice vestibular system.

Experimental investigation

Materials and Methods

Tissue preparation

Animal procedures were performed at the University of Sheffield (UK) and at the University of Pavia (Italy) according to the local dispositions.

Experiments were performed on both male and female mice and ranging from postnatal day 4 (P4) to P35. $Ca_v1.3$ knockout mice ($Ca_v1.3^{-/-}$) were obtained by C57BL/6N background, also control mice were littermate heterozygous or C57BL/6N.

The semicircular canals with their *ampullae* were dissected out from the inner ear as reported below.

After cervical dislocation, the cranium was sectioned in two halves along the sagittal plane, the brain removed, and the bony labyrinth located. In order to preserve cell viability, half heads were transferred in a Petri dish filled with chilled extracellular solution (Extra_std, in mM): 135 NaCl, 5.8 KCl, 1.3 $CaCl_2$, 0.9 $MgCl_2$, 0.7 NaH_2PO_4, 5.6 D-glucose, 10 HEPES-NaOH. Sodium pyruvate (2 mM), amino acids and vitamins were added from concentrates (Thermo Fisher Scientific, UK). The pH was adjusted to 7.5 (osmolality ~308 mmol kg^{-1}).

To isolate the *ampullae*, surgical dissection was continued under a stereomicroscope (Leica MZ95). First, the temporal bone covering the anterior and lateral *ampullae* was removed to expose the bony labyrinth. In order to allow access to the membranous labyrinth, the posterior semicircular canal was cut, and the remaining part of the bone was completely pulled out. So, the *ampullae* could be isolated. Successively, the ampulla roof was cut in order to expose the crista sensory epithelium. The dissected organs were then fixed at the bottom of the recording chamber by a nylon-meshed silver ring and were continuously perfused with the above extracellular solution (0.5 ml/min) using a peristaltic pump (Masterflex L/S, Cole Palmer, USA). Hair cells were viewed using a upright microscopes (Olympus BX51; Leica DM-LFS) equipped with Nomarski Differential Interface Contrast (DIC) optics with a 60X or 64X water immersion objective and x15 eyepieces.

The cochleae (apical turn) were dissected out from the inner ear as reported previously (Jeng et al., 2020).

Whole-cell electrophysiology

Voltage-clamp whole-cell experiments were performed at room temperature (18-22 °C) for K^+ current recordings, and near-body temperature (32-36 °C) for Ca^{2+} currents recordings using an Optopatch amplifier (Cairn Research Ltd, UK) as previously described (Johnson and Marcotti, 2008; Jeng et al. 2020b; Spaiardi et al., 2020b). The patch pipettes were pulled to 2-3 MΩ tip resistance from soda glass capillaries (Hilgenberg, Germany) and coated with surf-wax (Mr Zoggs SexWax, USA) to minimize the fast capacitance transient across the wall of the patch pipette. For K^+ current recordings, the patch pipette filling solution contained (in mM): KCl 131, Na_2-Phosphocreatine 10, $MgCl_2$ 3, EGTA-KOH 1, Na_2ATP 5 and HEPES 5; pH adjusted to 7.28 with KOH (osmolality was 294 mmol kg^{-1}). For Ca^{2+} current recordings, the pipette intracellular solution contained (in mM): 106 Cs-glutamate, 20 CsCl, 3 $MgCl_2$, 1 EGTA-CsOH, 5 Na_2ATP, 0.3 Na_2GTP, 5 HEPES-CsOH, 10 Na_2-phosphocreatine, pH 7.3 with CsOH (294 mmol kg^{-1}). Data acquisition was controlled by pClamp software using a Digidata board (Molecular Devices, USA). Recordings were low-pass filtered at either 2.5 or 5 kHz (8-pole Bessel), sampled at 5, 10 or 100 kHz and stored on computer for off-line analysis using Clampfit (Molecular Devices, USA) and Origin (OriginLab, USA) software. Membrane potentials reported in the text and figures were corrected for the uncompensated residual series resistance (Rs) and the liquid junction potential (LJP), which was either –4 mV for the K^+-based and –11 mV for the Cs^+-glutamate-based intracellular solution, measured between electrode and bath solutions. For K^+ current recordings from vestibular hair cells, Rs was calculated off-line from the capacitive artifact elicited by applying a voltage step from either –74 mV to –64 mV in type II and –124 mV to –44 mV in type I hair cells. The different voltage step was used in order to minimize artifact contamination by inward and outward rectifier voltage-gated channels in the two hair cell types (Spaiardi et al., 2017). Voltage clamp protocols are referred to a holding potential of –64 mV for the K^+-based intracellular solution or –91 mV for the Cs^+-based intracellular solution.

For Ca^{2+} current recordings, the composition of the extracellular solution contained (in mM): NaCl 101, $CaCl_2$ 5, CsCl 5.8, $MgCl_2$ 0.9, HEPES 10, glucose 5.6, tetraethylammonium (TEA) 30, 4-aminopyridine (4AP) 15 (pH adjusted with HCl was 7.5; osmolality: 312 mOsm/kg). The higher Ca^{2+} concentration (5 mM) was used to better visualize the Ca^{2+} current in $Ca_V1.3^{-/-}$ mice. Extracellular TEA, 4-AP and intracellular Cs^+ (see above) were used to block the K^+ channels (cochlear IHCs: Marcotti et al., 2003 Pt 2, Jeng et al., 2020b, Jeng et al., 2021; vestibular hair cells: Rennie and Correia, 1994; Biel et al., 2009). Moreover, the K^+ channel

blockers linopirdine (80 μM; Tocris, UK) was also used to block $I_{K,n}$ in adult IHCs (Marcotti et al., 2003 Pt 2). In some experiments, $CdCl_2$ 0.1 mM was also added to the above extracellular solution to block the Ca^{2+} current (Hille, 2001) in vestibular hair cells. The amplitude of the Ca^{2+} current was measured by either subtracting the linear leakage current component, measured between –81 mV and –91 mV, or the current blocked by Cd^{2+} from the current recorded in the presence of TEA and 4-AP (see above).

Data analysis

Statistical comparisons of means were made by Student's two-tailed t-test or, for multiple comparisons, analysis of variance (one way or two-way ANOVA) was applied. $P<0.05$ was selected as the criterion for statistical significance. Mean values are quoted as means ± SD.

Results

Potassium currents recorded from Type I and Type II crista hair cells from control and $Ca_v1.3^{-/-}$ mice

Mammalian vestibular type I and type II hair cells can be distinguished by the expression of a large low-voltage activated outward rectifying K^+ currents, named $I_{K,L}$ (Rennie and Correia, 1994; Rüsch and Eatock, 1996). In figure 13A, B it is reported whole-cell current recordings from vestibular Type I hair cells (P17-22) of wild-type (Fig.13A) and $Ca_v1.3^{-/-}$ mice (Fig.13B). Since $I_{K,L}$ is almost completely activated at –60 mV, hyperpolarizing voltages from the holding potential of –64 mV produced deactivating tail currents (*e.g.* –104 mV and –124 mV: Fig.13A, B), while depolarizations elicit an instantaneous increase of the outward currents. In figure 13C it is shown the mean steady-state current-voltage (I-V) relations of the macroscopic inward and outward rectifying K^+ currents in wild-type (P17-P22; n = 12) and $Ca_v1.3^{-/-}$ mice (P19-P20; n = 6) from Type I hair cells. The amplitude of the inward and outward rectifying K^+ currents in KO cells was not significantly different from that measured in WT cells (P = 0.9742, F = 0.4149, DFn = 15, two-way ANOVA).

The negligible steady-state current at –124 mV is consistent with $I_{K,L}$ being fully deactivated at this potential, and with the absence of inward rectifier currents in mouse *crista* type I hair cells (Spaiardi et al., 2020a). Note that the outward tail currents in type I hair cells, which were recorded at –44 mV, were smaller following the voltage step to –24 mV than those at –44 mV in both wild-type (Fig.13A, D) and $Ca_v1.3^{-/-}$ mice (Fig.13B, E, F). The presence of progressively smaller outward tail current following larger outward K^+ currents, which in some cases includes tail current reversal (Fig.13F), is consistent with intercellular (*e.g.*, in the calyceal synaptic cleft) K^+ accumulation inducing a shift in the K^+ equilibrium potential (Lim et al., 2011; Contini et al., 2012; Contini et al., 2017; Spaiardi et al., 2020a; Contini et al., 2020). Progressive intercellular K^+ accumulation during depolarization is also responsible for the "apparent" inactivation of the outward current, which is due to the progressive decrease of the driving force for K^+ to exit the hair cells (*e.g.*, Spaiardi et al., 2017).

Different from the type I hair cells, the adult type II hair cells are not dominated by $I_{K,L}$ (Fig.13G, H), but are dominated by a transient outward current ($I_{K,A}$) and a delayed and sustained outward current ($I_{K,v}$) activates following depolarization. Instead the hiperpolarization activates an inward rectifying K^+ current ($I_{K,1}$) and the mixed inward rectifying Na^+/K^+ current (I_h).

All these currents were evident from the inward and outward current profile recorded from type II hair cells of both wild-type and $Ca_v1.3^{-/-}$ mice. The mean steady-state *I-V* for the total current recorded in type II hair cells was also not significantly different between wild-type (P17-P22; n = 4) and $Ca_v1.3^{-/-}$ mice (P18-P19; n = 4) ($P = 0.7010$, $F = 0.7756$, DFn = 15, two-way ANOVA, Fig.13I).

These results indicate that the loss of the $Ca_v1.3$ Ca^{2+} channel subunit does not affect the K^+ current properties in vestibular type I and II hair cells in the *crista*. This is different from the cochlea, where the normal expression of the K^+ currents characteristic of IHCs, which are the fast activating current $I_{K,f}$ and negatively activating delayed rectifier $I_{K,n}$ (Kros et al., 1998; Marcotti et al., 2003 Pt 2; Oliver et al., 2003), was either prevented (apical-coil) or reduced (basal-coil) in $Ca_v1.3^{-/-}$ mice (Brandt et al., 2003; Jeng et al., 2020a).

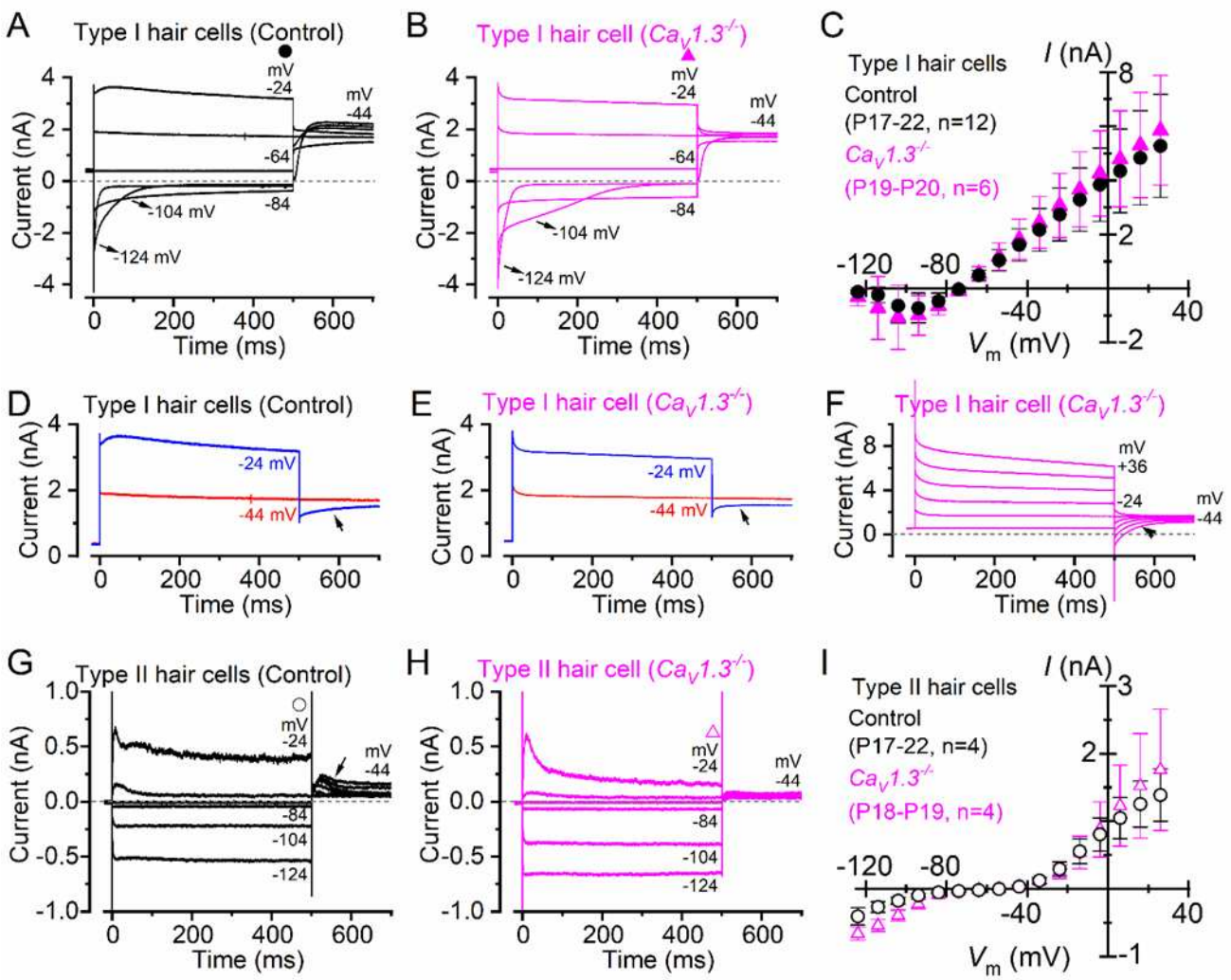

Figure 13. Type I and type II crista hair cells express normal K^+ currents in control and $Ca_v1.3^{-/-}$ adult mice.
(A), (B), Membrane current responses from type I hair cells of control (A, P18) or $Ca_v1.3^{-/-}$ (B, P20) adult mice were performed by applying 500 ms depolarizing voltage steps of 10 mV nominal increment from –124 mV, starting from a holding potential of –64 mV. For clarity, only a few test potentials are shown. C, Steady-state current-voltage (I-V) curves obtained from type I hair cells of control (P17-22) and $Ca_v1.3^{-/-}$ (P19-20) mice. (D), (E), Current responses from panels A and B, but at only two membrane potentials that better emphasize the tail currents. (F), Potassium current recorded from a type I hair cell of a $Ca_v1.3^{-/-}$ mouse (P19). The tail currents at –44 mV were elicited following 500 ms voltage steps between -64 mV to 40 mV in 20 mV nominal increments (actual membrane potential is shown near some of the traces). The instantaneous tail currents reverse (arrow) following the two most depolarized voltage steps. The horizontal dashed line represents the zero-current level. For a detailed explanation of the above phenomenon see: Spaiardi et al., 2017. (G), (H), The rapid inactivation of the current responses from type II hair cells of control (G, P17) or $Ca_v1.3^{-/-}$ (H, P19) adult mice obtained using the voltage protocol described above. Note that the larger tail outward currents at –44 mV (arrow in G), elicited following the 500 ms hyperpolarizing voltage steps, were due to progressive removal of $I_{K,A}$ inactivation. (I), Steady-state current-voltage (I-V) curves obtained from type II hair cells of control (P17-22) and $Ca_v1.3^{-/-}$ (P18-19) mice. In panel C and I, values are shown as mean ± S.D.

Calcium currents in Type I and Type II hair cells in control and $Ca_v1.3^{-/-}$ mice

It is difficult to distinguish morphologically type I from type II hair cells when working with the intact organ. Therefore, the correct identification of type I hair cells relies on the presence of $I_{K,L}$ (Fig.13) and for its state of deactivation at the holding potential used for the recordings, which is set at –90 mV. Recordings were performed using intracellular Cs^+, which is known to block I_h (Biel et al., 2009) and the outward rectifying K^+ currents (Bao et al., 2003) in type II hair cells while having little effects on $I_{K,L}$ (Griguer et al., 1993; Rüsch and Eatock, 1996; Chen and Eatock, 2000; Rennie and Correia, 2000). Fig.14A, C shows a large deactivation at -91 mV and a small instantaneous current upon depolarizing and hyperpolarizing voltage steps. In the example shown in figure14B, C, however, $I_{K,L}$ is largely activated at –91 mV and exhibits large instantaneous currents. Although this variability has previously been reported (Hurley et al., 2006; Spaiardi et al., 2017), we found that the reversal potential for the macroscopic current was significantly more hyperpolarised in type I hair cells showing a largely activated $I_{K,L}$ at –91 mV (Fig.14C). In figure 14D it is shown the correlation between the age and the level of deactivation of $I_{K,L}$, which is largely pronounced in early postnatal hair cells (n = 15), then more mature cells (n = 8). The reversal potential of the macroscopic K^+ current in type I hair cells should reach values near the reversal potential of the mixed Cs^+/K^+ current (called a ‘‘biionic potential”, see Hille, 2001) through K,L channels. (Spaiardi et al., 2020a). Given the reported permeability ratio of Cs^+ to K^+ of about 0.31 (Rüsch and Eatock, 1996; Spaiardi et al., 2020a), the reversal potential should be close to –40 mV. The finding that the reversal potential in older hair cells (Fig.14C) is close to –60 mV could indicate that the relative permeability of K,L channels to Cs^+ is likely to be larger than that previously estimated, at least in more mature type I hair cells. However, the presence of a residual calyx might also produce a shift of the mixed Cs^+/K^+ equilibrium potential towards more negative voltages during inward currents (Spaiardi et al., 2017; Spaiardi et al., 2020a). This would imply a tighter attachment of the calyx to more mature type I hair cells.

The above results are consistent with $I_{K,L}$ increasing in amplitude and activating at more hyperpolarized potentials during post-natal development, as also previously shown in rat type I hair cells (Hurley et al., 2006). Different K^+ channels subunits have also been found to be expressed by rodent type I hair cells during postnatal development which may account for the above changes (Hurley et al., 2006; Spitzmaul et al., 2013).

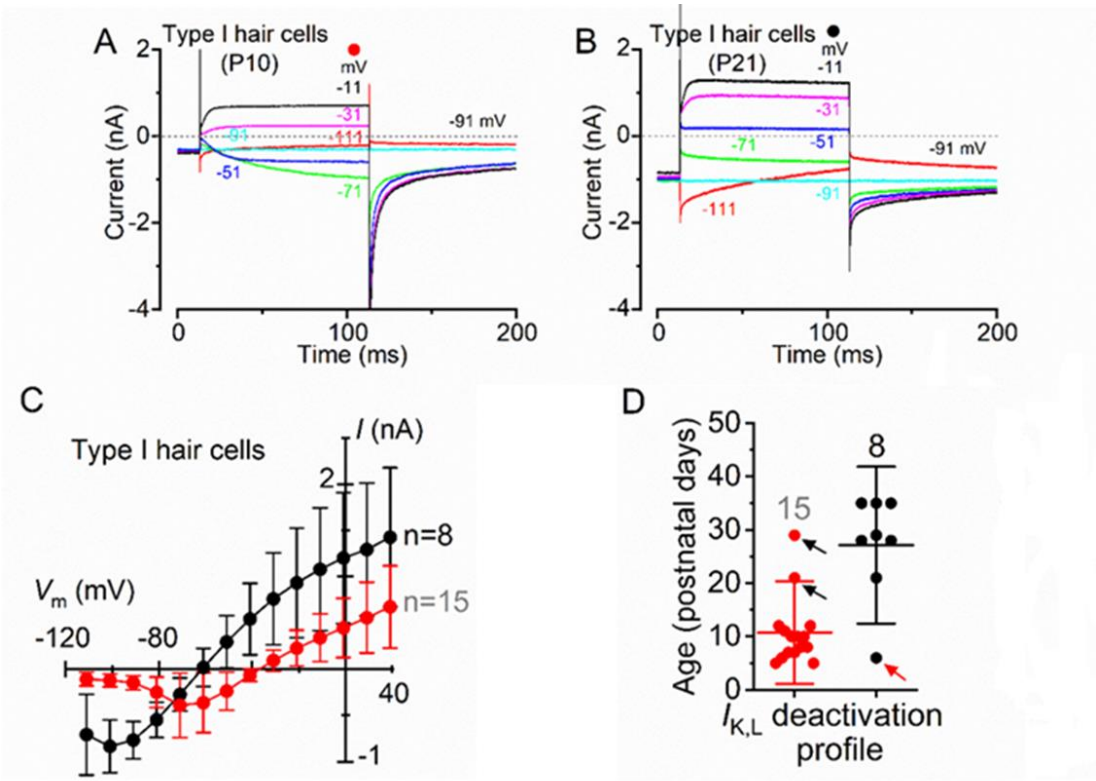

Figure 14. Type I crista hair cells can be identified by their large permeability to Cs^+ in wild-type neonatal and adult mice. (A), (B), Representative membrane current responses recorded from type I hair cells of control mice of different age with Cs^+ as main ion carrier in the intracellular solution (A, P10; B, P21). Currents were elicited by 500 ms depolarizing voltage steps of 10 mV nominal increment from –111 mV starting from a holding potential of –91 mV. For clarity, only a few test potentials are shown. (C), Steady-state current-voltage (I-V) curves obtained from type I hair cells arbitrarily subdivided into two groups depending if the inward current through the K,L channels was (red), or was not (black), completely deactivated at –111 mV. Values are shown as mean ± SD. (D), Age distribution of type I hair cells expressing $I_{K,L}$ that was (red), or was not (black), completely deactivated at –111 mV. Each symbol refers to the steady-state value of $I_{K,L}$ measured in each cell at –111 mV.

Following the positive identification of the patched hair cell as type I, the addition of the K^+ channel blockers (TEA and 4AP) in the presence of 5 mM Ca^{2+} (see Methods) allowed to detect a small inward current (Fig.15A, upper panel). In a subset of type I hair cells (n = 8) of $Ca_v1.3^{+/+}$mice, we found that the addition of 0.1 mM Cd^{2+} to the extracellular solution fully blocked the inward current, confirming its identity as I_{Ca} (Fig.15A, lower panel). The isolated I_{Ca} was obtained by subtracting the current recorded in the presence of TEA, 4AP and Cd^{2+} to that obtained in the absence of Cd^{2+} (Fig.15B). Average values of peak I_{Ca} amplitude were measured at each voltage steps and plotted against voltage (Fig.15D). As shown in figure the inward current activated at about −61 mV and peaked near −21 mV (Fig.15D). We also

considered it was appropriate to subtract the leakage from current recorded in TEA and 4AP, so this procedure provided the same isolated I_{Ca} as that following the subtraction (Fig.15C, D). In $Ca_v1.3^{-/-}$ mice, the inward current was barely visible in type I hair cells when the extracellular solution contained TEA, 4AP and 5 mM Ca^{2+} (Fig.15E). Also in this case, the isolated I_{Ca} was obtained by subtracting the current recorded in extracellular TEA, 4AP and 0.1 mM Cd^{2+} to that recorded in TEA and 4AP (Fig.15F). The inward current activated at about -40mV and peaked near −11 mV (Fig.15H). Comparable results were obtained when I_{Ca} was isolated by performing the leakage-subtraction procedure (Fig.15G). In type I hair cells, the mean peak I_{Ca} after Cd^{2+}-subtraction was 121 pA in wild-type and 19 pA in $Ca_v1.3^{-/-}$ mice (15.7% of the wilt-type value) (Fig.15D, H)

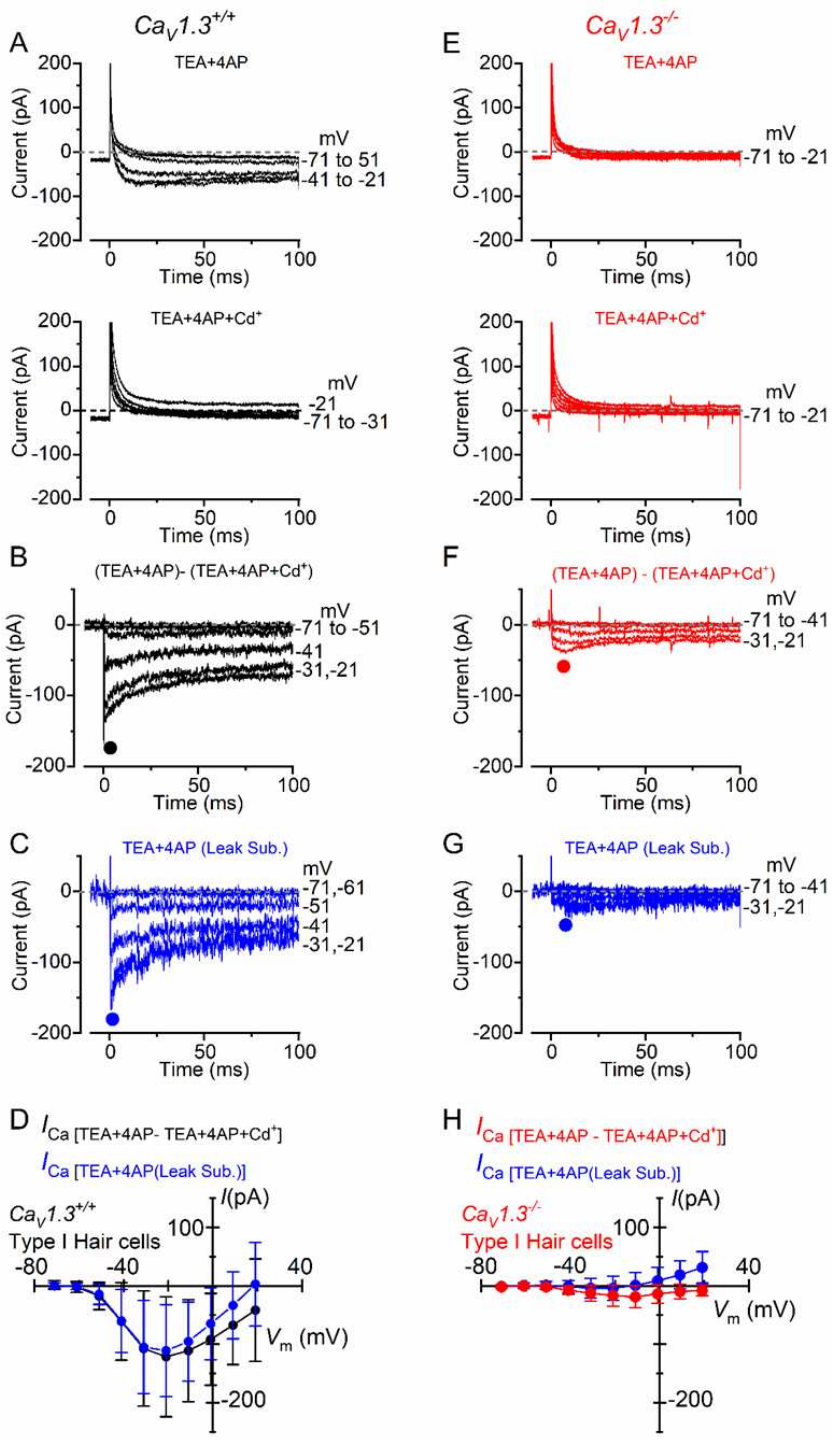

Figure 15. Calcium currents in type I crista hair cells from wild-type and $Ca_V1.3^{-/-}$ mice.
(A), Inward current recorded from a type I hair cell of a wild-type mouse (P5, upper panel) in the presence of 30 mM TEA and 15 mM 4AP in the extracellular solution and Cs^+ as the main ion carrier in the intracellular solution. Currents were elicited by 100 ms depolarizing voltage steps of 10 mV nominal increment (holding potential of –91 mV). For clarity, only a few test potentials are shown. Lower panel: inward current recorded from the same cell and solution shown in the top panel but with the additional 0.1 mM Cd^{2+} (Ca^{2+} channel blocker). (B), Inward Ca^{2+} current from the same wild-type hair cell shown in A obtained by subtracting the current recorded in extracellular TEA, 4AP and 0.1 mM Cd^{2+} to that recorded in TEA and 4AP. (C), Inward current obtained by leakage subtraction of the current recorded from the cell in A, upper panel. (D), Peak inward I-V curves for the current obtained as the Cd^{2+}-sensitive current (black symbols, n = 8) or after leakage subtraction (blue symbols; n = 17). (E), (F), (G) Inward currents recorded from a type I hair cell from a $Ca_V1.3^{-/-}$ (P5) mouse obtained as described in panel A, B, and C. (H), Peak inward I-V curves for the current obtained as the Cd^{2+}-sensitive current (red symbols, n = 10) or after leakage subtraction (blue symbols; n = 36). Values in panels D and H are shown as mean ± SD.

The isolation of the inward current in type II hair cells was performed using the same procedure as for Type I hair cells. In figure 16A and D are shown I_{Ca}, using either the isolated Cd^{2+}-procedure (Fig.16A and D) or after leakage subtraction (Fig.16B and E) in both wild-type and $Ca_v1.3^{-/-}$ mice. The amplitude of the Cd^{2+}-sensitive current (I_{Ca}: Fig.16A, C) was not significantly different to that obtained by leakage-subtraction (Fig. 16B, P <0.9336, F = 0.3916, DFn = 9, two-way ANOVA), or to the Cd^{2+}-sensitive current measured in wild-type type I hair cells (Fig.15B, D: P <0.8457, two-way ANOVA). The size of the Cd^{2+}-sensitive I_{Ca} recorded in type II hair cells of $Ca_v1.3^{-/-}$ mice (Fig.16D, E, F), was very similar to that measured in type I hair cells (Fig.15F, G, H, P <0.7677, F = 0.6319, DFn = 9, two-way ANOVA), both in the presence of TEA and 4AP after leakage subtraction (n = 12) or after its isolation with Cd^{2+}. In type II hair cells, the mean peak I_{Ca} after Cd^{2+}-subtraction was 142 pA in wild-type and 27 pA in $Ca_v1.3^{-/-}$ mice (19.0% of the wilt-type value).

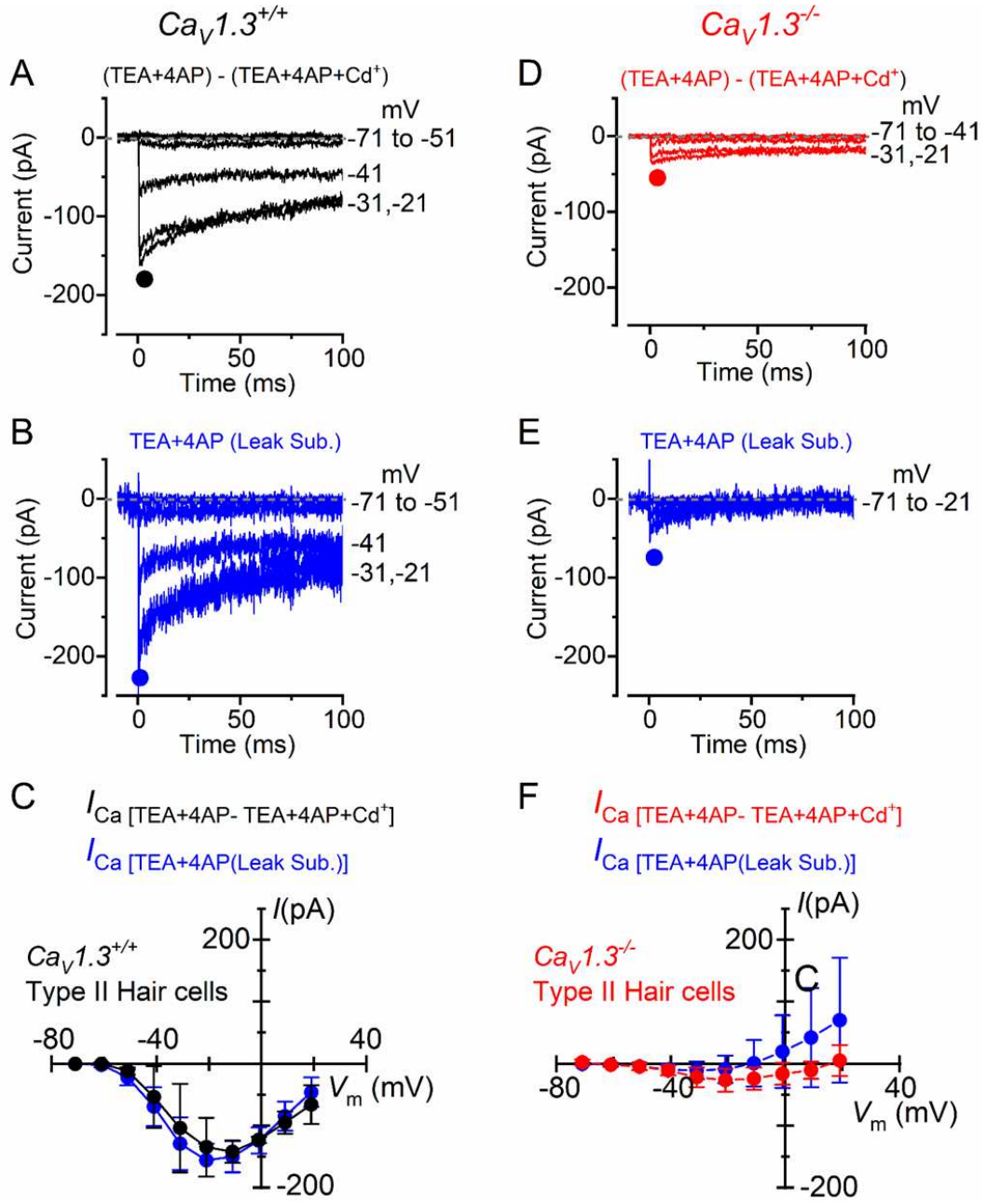

Figure 16. Calcium currents in type II crista hair cells from wild-type and $Ca_V1.3^{-/-}$ mice.
(A), (B), Inward current recorded from a type II hair cell of a wild-type mouse (P5) using the same experimental conditions described in figure 15B and C. For clarity, only a few test potentials are shown. (C), Peak inward I-V curves for the Cd^{2+}-sensitive current (black symbols, n = 2) or for the current after leakage subtraction (blue symbols; n = 5). (D), (E) Inward currents recorded from a type II hair cell from a $Ca_V1.3^{-/-}$ (P5) mouse obtained as described in panel A and B. (F), Peak inward I-V curves for the current obtained as the Cd^{2+}-sensitive current (red symbols, n = 3) or after leakage subtraction (blue symbols; n = 12). Values in panels C and F are shown as mean ± SD.

To assess that the age did not affect the size of I_{Ca}, the peak amplitude (between -21 and -11 mV) has been related to postnatal ages. The figure 17 shows that there were no differences in both type I and type II hair cells between early and late postnatal ages from wild-type and $Ca_v1.3^{-/-}$ mice.

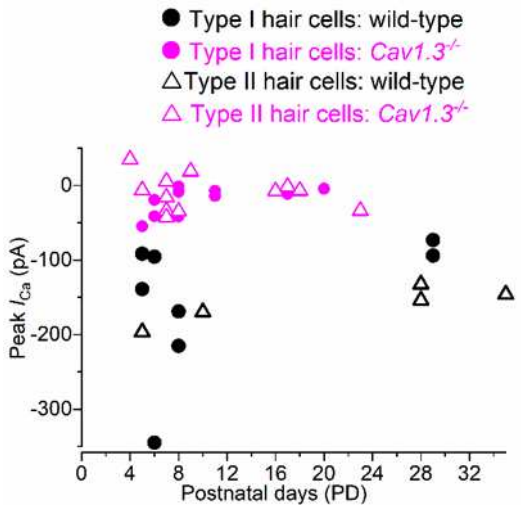

Figure 17. Calcium current in type I and type II hair cells as a function of postnatal age in mice.
Peak of the Ca^{2+} current measured as a function of postnatal age in type I and type II hair cells from both wild-type and $Ca_v1.3^{-/-}$ mice. Single data points are shown.

Calcium currents in the Inner Hair Cells (IHCs) of the mouse cochlea from $Ca_v1.3^{-/-}$ mice

The same solutions (intracellular Cs^+, extracellular TEA and 4AP and 5 mM Ca^{2+}) and temperature conditions (32-36 ºC) have been used to investigate ICa in cochlear IHCs (Fig.18). Data obtained underline how about 10% of the total ICa in apical IHCs is carried by Ca^{2+} channels other than $Ca_v1.3$ (Platzer et al., 2000; Michna et al., 2003). The size of ICa, measured after leakage-subtraction, was largely reduced in IHCs from $Ca_v1.3^{-/-}$ mice compared to littermate controls at both immature ($P < 0.0001$, $F = 63.70$, $DFn = 9$) and adult ages (Fig.18G, $P < 0.0001$, $F = 20.33$, $DFn = 9$, between the same voltage range used for the vestibular hair cells: -61 to +29 mV, two-way ANOVA). The residual current observed in cochlear hair cells is comparable to vestibular hair cells. The nature of Ca^{2+}channels responsible of this current are unknown; previous suggestions indicated the presence of $Ca_v1.4$ in both immature and adult IHCs (Brandt et al., 2003) and of $Ca_V3.1$ T-type subunits in immature avian auditory hair cells (Levic et al., 2012).

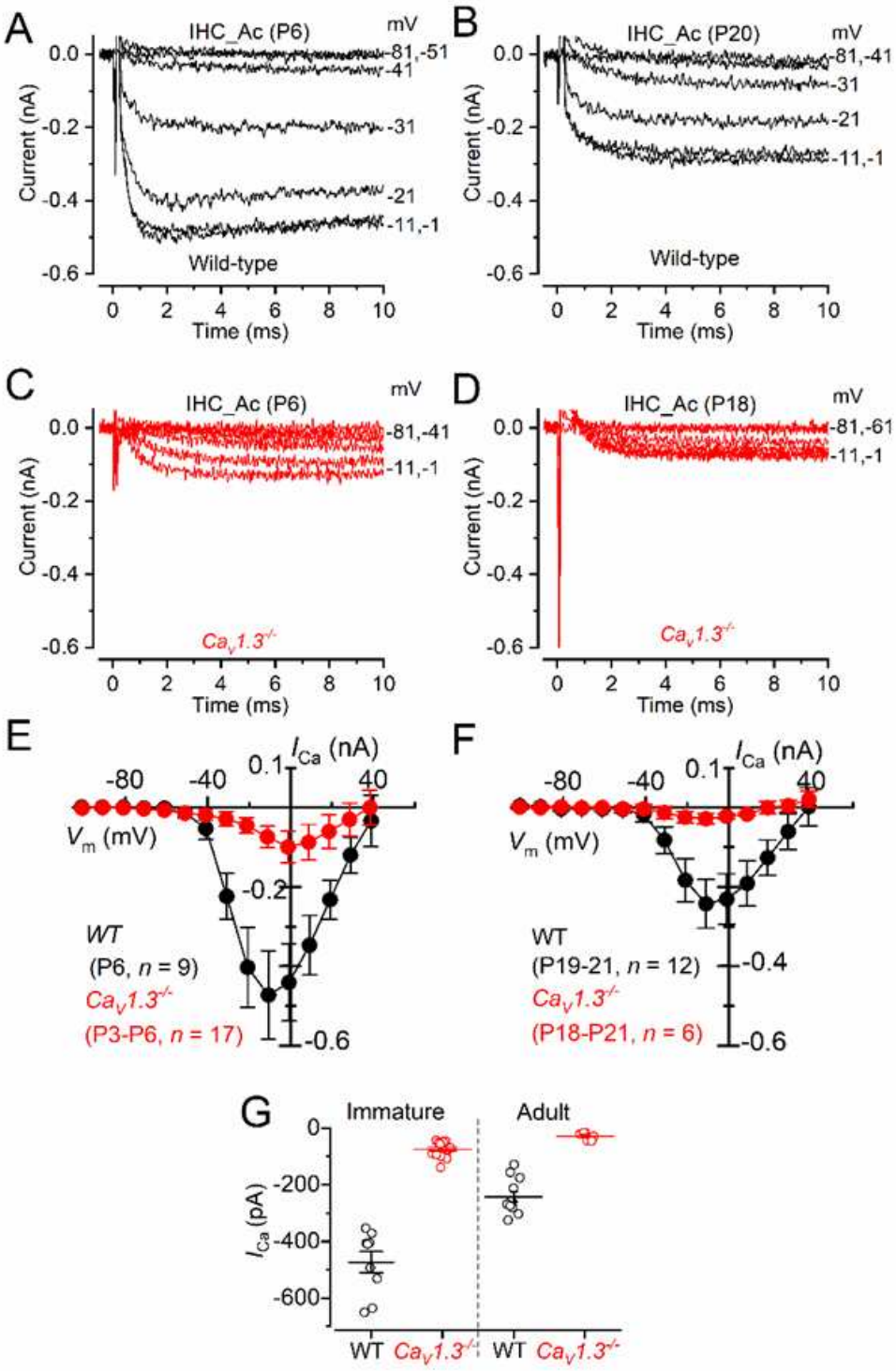

Figure 18. Calcium currents in IHCs from $Ca_V1.3^{-/-}$ mice.
(A), (B), Calcium currents recorded from immature (A, P6) and adult (B, P20) IHCs of wild-type mice. Currents were elicited by depolarizing voltage steps of 10 mV increments (10 ms in duration) starting from the holding potential of –81 mV. (C), (D), Calcium currents from immature (C, P6) and adult (D, P18) IHCs of $Ca_V1.3^{-/-}$ mice. For clarity, in panels A-D only some of the traces are shown. Actual test potentials, corrected for voltage drop across uncompensated R_s, are shown next to the traces. (E), (F), Current-voltage relationship for the inward Ca^{2+} current in immature (E) and adult (F) IHCs from both wild-type and $Ca_V1.3^{-/-}$ mice. (G), Peak Ca^{2+} current in both genotypes at immature and adult IHCs. One-way ANOVA (overall: P<0.0001, F = 98.98, DFn = 43) Tukey's post-test analysis: wild-type immature (-473 ± 112 pA, n = 9) vs. $Ca_V1.3^{-/-}$ immature (-74 ± 27 pA, n = 17), P<0.0001; wild-type adult (-243 ± 61 pA, n = 12) vs. $Ca_V1.3^{-/-}$ adult (-28 ± 14 pA, n = 6), P<0.001; wild-type immature vs. wild-type adult, P<0.001; wild-type immature vs. $Ca_V1.3^{-/-}$ adult, P<0.001; $Ca_V1.3^{-/-}$ immature vs. wild-type adult, P<0.001; $Ca_V1.3^{-/-}$ immature vs. $Ca_V1.3^{-/-}$ adult, P>0.05. Data are reported as mean ± SD.

Discussion

The present study demonstrated that, compared to what was seen in cochlea hair cells, the mature K^+ current in the crista hair cells was not dependent on the presence of $Ca_v1.3$ Ca^{2+} channels; indeed, type I and type II hair cells from $Ca_v1.3^{-/-}$ mice were able to acquire the adult-like K^+ current profile in their basolateral membrane.

Moreover, we compared the level of expression of the Ca^{2+} current in hair cells of the crista and cochlear IHCs from wild-type and $Ca_v1.3^{-/-}$ mice and we found that the residual Ca^{2+} current was only <20% to that of control cells.

It is known that cochlea express adult-like K^+ channels, which activity is regulated by Ca^{2+} dependent action potentials during pre-hearing stages. IHCs and OHCs from pre-hearing $Ca_v1.3^{-/-}$ mice, which are unable to elicit Ca^{2+} action potentials, retain an immature K^+ current profile even at adult stages (Brandt et al., 2003; Ceriani et al., 2019; Jeng et al., 2020a). However, vestibular hair cells seem not to elicit action potentials during early postnatal developmental stages. This explains how the absence of the $Ca_v1.3$ Ca^{2+} current does not influence the maturation of vestibular hair cells.

When $Ca_v1.3$ Ca^{2+} channels are not expressed, both mice (Platzer et al., 2000; Dou et al., 2004) and humans (Baig et al., 2011) suffer with deafness, but without showing any visible vestibular dysfunctions; in addition, the absence of Ca^{2+}-dependent exocytosis in hair cells doesn't suppress or reduce the vestibular function.

Tests such as vestibular evoked potentials (VsEPs) are necessary in order to reveal subtle vestibular impairments (Jones and Jones, 2014) because partial vestibular compensation may occur by other sensory systems.

Moreover, the lack of otoferlin, a synaptic protein present in cochlear and vestibular hair cells, causes deafness in mice, but not abnormal posturing, imbalance or nystagmus (Roux et al., 2006) although subtle vestibular dysfunctions can be unveiled by VsEPs (Dulon et al., 2009).

The $Ca_v1.3$ subunit is responsible for the majority current both in cochlear and vestibular hair cells, a small residual Ca^{2+} current (<20%) is visible from IHCs, type I, type II hair cells in Cav $1.3^{-/-}$ mice.

This result disagrees with a study performed on early postnatal hair cells from the utricle of $Ca_v1.3^{-/-}$ mice (P1-P10: Dou et al., 2004) which showed about 50% of residual inward Ba^{2+} current through voltage-gated Ca^{2+} channels.

Since we observed a similar residual Ca^{2+} current in both neonatal and adult vestibular hair cells from $Ca_v1.3^{-/-}$ mice, the age difference doesn't count. An alternative explanation is that the expression level of the $Ca_v1.3$ subunit is different between utricle and crista hair cells.

In principle, the remaining Ca^{2+} channels in some type I and type II vestibular hair cells might be able to drive some exocytosis in order to reduce anomalous vestibular phenotype in $Ca_v1.3^{-/-}$ mice.

An attractive possibility for the absence of an anomalous vestibular phenotypes in $Ca_v1.3^{-/-}$ mice, however, is likely to be associated with the presence of non-quantal synaptic transmission in vestibular type I hair cells, but not cochlear IHCs (Yamashita and Ohmori, 1990; Holt et al., 2007; Songer and Eatock, 2013). This non-conventional, K^+-based synaptic transmission relays on intercellular K^+ increase in the extended narrow synaptic cleft between the basolateral membrane of type I hair cells and the inner face of the afferent calyx terminal (Lim et al., 2011; Contini et al., 2012; Contini et al., 2017; Spaiardi et al., 2020a) and fast, direct resistive coupling between pre- and postsynaptic K^+ channels facing the synaptic cleft (Contini et al., 2020).

From this study it was found that $I_{K,L}$, which is normally present in $Ca_v1.3^{-/-}$ mice, plays a major role in this K^+-based signal transmission at the calyx synapse (Contini et al., 2017; Eatock, 2018) (Fig.13).

In addition, intercellular K^+ increase occurs in $Ca_v1.3^{-/-}$ mice, suggesting that calyces develop normally around the type I hair cell basolateral membrane.

In conclusion, the presence of this K^+-based afferent transmission, which is unlikely to be affected in $Ca_v1.3^{-/-}$ mice, might contribute to the absence of obvious vestibular dysfunction in these mice.

References

- Ahmed ZM, Goodyear R, Riazuddin S, Lagziel A, Legan PK, Behra M, Burgess SM, Lilley KS, Wilcox ER, Riazuddin S, Griffith AJ, Frolenkov GI, Belyantseva IA, Richardson GP, Friedman TB. The tip-link antigen, a protein associated with the transduction complex of sensory hair cells, is protocadherin-15. J Neurosci. 2006 Jun 28;26(26):7022-34. doi: 10.1523/JNEUROSCI.1163-06.2006. PMID: 16807332; PMCID: PMC6673907.

- Baig SM, Koschak A, Lieb A, Gebhart M, Dafinger C, Nürnberg G, Ali A, Ahmad I, Sinnegger-Brauns MJ, Brandt N, Engel J, Mangoni ME, Farooq M, Khan HU, Nürnberg P, Striessnig J, Bolz HJ. Loss of Ca(v)1.3 (CACNA1D) function in a human channelopathy with bradycardia and congenital deafness. Nat Neurosci. 2011 Jan;14(1):77-84. doi: 10.1038/nn.2694. Epub 2010 Dec 5. PMID: 21131953.

- Bao H, Wong WH, Goldberg JM, Eatock RA. Voltage-gated calcium channel currents in type I and type II hair cells isolated from the rat crista. J Neurophysiol. 2003 Jul;90(1):155-64. doi: 10.1152/jn.00244.2003. Erratum in: J Neurophysiol. 2004 Jan;91(1):589. PMID: 12843307.

- Baumann L, Gerstner A, Zong X, Biel M, Wahl-Schott C. Functional characterization of the L-type Ca^{2+} channel $Ca_v1.4alpha1$ from mouse retina. Invest Ophthalmol Vis Sci. 2004 Feb;45(2):708-13. doi: 10.1167/iovs.03-0937. PMID: 14744918.

- Bernard C, Ferrary E, Sterkers O. Production of endolymph in the semicircular canal of the frog Rana esculenta. J Physiol. 1986 Feb; 371:17-28. doi: 10.1113/ jphysiol. 1986. sp015959. PMID: 3486270; PMCID: PMC1192708.

- Beurg M, Fettiplace R, Nam JH, Ricci AJ. Localization of inner hair cell mechanotransducer channels using high-speed calcium imaging. Nat Neurosci. 2009 May;12(5):553-8. doi: 10.1038/nn.2295. Epub 2009 Mar 29. PMID: 19330002; PMCID: PMC2712647.

- Beurg M, Michalski N, Safieddine S, Bouleau Y, Schneggenburger R, Chapman ER, Petit C, Dulon D. Control of exocytosis by synaptotagmins and otoferlin in auditory hair cells. J Neurosci. 2010 Oct 6;30(40):13281-90. doi: 10.1523/JNEUROSCI.2528-10.2010. PMID: 20926654; PMCID: PMC3088501.

- Beutner D, Moser T. The presynaptic function of mouse cochlear inner hair cells during development of hearing. J Neurosci. 2001 Jul 1;21(13):4593-9. doi: 10.1523/JNEUROSCI.21-13-04593.2001. PMID: 11425887; PMCID: PMC6762371.

- Biel M, Wahl-Schott C, Michalakis S, Zong X. Hyperpolarization-activated cation channels: from genes to function. Physiol Rev. 2009 Jul;89(3):847-85. doi: 10.1152/physrev.00029.2008. PMID: 19584315.

- Bird JE, Daudet N, Warchol ME, Gale JE. Supporting cells eliminate dying sensory hair cells to maintain epithelial integrity in the avian inner ear. J Neurosci. 2010 Sep 15;30(37):12545-56. doi: 10.1523/JNEUROSCI.3042-10.2010. PMID: 20844149; PMCID: PMC2963157.

- Bock G, Gebhart M, Scharinger A, Jangsangthong W, Busquet P, Poggiani C, Sartori S, Mangoni ME, Sinnegger-Brauns MJ, Herzig S, Striessnig J, Koschak A. Functional properties of a newly identified C-terminal splice variant of $Ca_v1.3$ L-type Ca^{2+} channels. J Biol Chem. 2011 Dec 9;286(49):42736-42748. doi: 10.1074/jbc.M111.269951. Epub 2011 Oct 13. PMID: 21998310; PMCID: PMC3234942.

- Brandt A, Khimich D, Moser T. Few $Ca_v1.3$ channels regulate the exocytosis of a synaptic vesicle at the hair cell ribbon synapse. J Neurosci. 2005 Dec 14;25(50):11577-85. doi: 10.1523/JNEUROSCI.3411-05.2005. PMID: 16354915; PMCID: PMC6726013.

- Brandt A, Striessnig J, Moser T. $Ca_v1.3$ channels are essential for development and presynaptic activity of cochlear inner hair cells. J Neurosci. 2003 Nov 26;23(34):10832-40. doi: 10.1523/JNEUROSCI.23-34-10832.2003. PMID: 14645476; PMCID: PMC6740966.

- Brichta AM, Peterson EH. Functional architecture of vestibular primary afferents from the posterior semicircular canal of a turtle, Pseudemys (Trachemys) scripta elegans. J Comp Neurol. 1994 Jun 22;344(4):481-507. doi: 10.1002/cne.903440402. PMID: 7929889.

- Buraei Z, Yang J. The ß subunit of voltage-gated Ca^{2+} channels. Physiol Rev. 2010 Oct;90(4):1461-506. doi: 10.1152/physrev.00057.2009. PMID: 20959621; PMCID: PMC4353500.

- Catterall WA, Few AP. Calcium channel regulation and presynaptic plasticity. Neuron. 2008 Sep 25;59(6):882-901. doi: 10.1016/j.neuron.2008.09.005. PMID: 18817729.

- Ceriani F, Hendry A, Jeng JY, Johnson SL, Stephani F, Olt J, Holley MC, Mammano F, Engel J, Kros CJ, Simmons DD, Marcotti W. Coordinated calcium signalling in cochlear sensory and non-sensory cells refines afferent innervation of outer hair cells. EMBO J. 2019 May 2;38(9): e99839. doi: 10.15252/embj.201899839. Epub 2019 Feb 25. PMID: 30804003; PMCID: PMC6484507.

- Chabbert C, Mechaly I, Sieso V, Giraud P, Brugeaud A, Lehouelleur J, Couraud F, Valmier J, Sans A. Voltage-gated Na^+ channel activation induces both action potentials in utricular hair cells and brain-derived neurotrophic factor release in the rat utricle during a restricted period of development. J Physiol. 2003 Nov 15;553(Pt 1):113-23. doi: 10.1113/jphysiol.2003.043034. Epub 2003 Sep 8. PMID: 12963806; PMCID: PMC2343473.

- Chen JW, Eatock RA. Major potassium conductance in type I hair cells from rat semicircular canals: characterization and modulation by nitric oxide. J Neurophysiol. 2000 Jul;84(1):139-51. doi: 10.1152/jn.2000.84.1.139. PMID: 10899192.

- Contini D, Holstein GR, Art JJ. Synaptic cleft microenvironment influences potassium permeation and synaptic transmission in hair cells surrounded by calyx afferents in the turtle. J Physiol. 2020 Feb;598(4):853-889. doi: 10.1113/JP278680. Epub 2019 Nov 29. PMID: 31623011; PMCID: PMC7024053.

- Contini D, Price SD, Art JJ. Accumulation of K^+ in the synaptic cleft modulates activity by influencing both vestibular hair cell and calyx afferent in the turtle. J Physiol. 2017 Feb 1;595(3):777-803. doi: 10.1113/JP273060. Epub 2016 Nov 4. PMID: 27633787; PMCID: PMC5285615.

- Contini D, Zampini V, Tavazzani E, Magistretti J, Russo G, Prigioni I, Masetto S. Intercellular K^+ accumulation depolarizes Type I vestibular hair cells and their associated afferent nerve calyx. Neuroscience. 2012 Dec 27; 227:232-46. doi: 10.1016/j.neuroscience.2012.09.051. Epub 2012 Sep 29. PMID: 23032932.

- Dallos P. The active cochlea. J Neurosci. 1992 Dec;12(12):4575-85. doi: 10.1523/JNEUROSCI.12-12-04575.1992. PMID: 1464757; PMCID: PMC6575778.

- Davis H. A model for transducer action in the cochlea. Cold Spring Harb Symp Quant Biol. 1965; 30:181-90. doi: 10.1101/sqb.1965.030.01.020. PMID: 5219471.

- DeRosier DJ, Tilney LG. The structure of the cuticular plate, an in vivo actin gel. J Cell Biol. 1989 Dec;109(6 Pt 1):2853-67. doi: 10.1083/jcb.109.6.2853. PMID: 2592408; PMCID: PMC2115895.

- Desai SS, Ali H, Lysakowski A. Comparative morphology of rodent vestibular periphery. II. Cristae ampullares. J Neurophysiol. 2005a Jan;93(1):267-80. doi: 10.1152/jn.00747.2003. Epub 2004 Jul 7. Erratum in: J Neurophysiol. 2021 Mar 1;125(3):781-783. PMID: 15240768.

- Desai SS, Zeh C, Lysakowski A. Comparative morphology of rodent vestibular periphery. I. Saccular and utricular maculae. J Neurophysiol. 2005b Jan;93(1):251-66. doi: 10.1152/jn.00746.2003. Epub 2004 Jul 7. PMID: 15240767.

- Dolphin AC. Calcium channel auxiliary α2δ and β subunits: trafficking and one step beyond. Nat Rev Neurosci. 2012 Jul 18;13(8):542-55. doi: 10.1038/nrn3311. PMID: 22805911.

- Dou H, Vazquez AE, Namkung Y, Chu H, Cardell EL, Nie L, Parson S, Shin HS, Yamoah EN. Null mutation of alpha1D Ca^{2+} channel gene results in deafness but no vestibular defect in mice. J Assoc Res Otolaryngol. 2004 Jun;5(2):215-26. doi: 10.1007/s10162-003-4020-3. PMID: 15357422; PMCID: PMC2538408.

- Dulon D, Safieddine S, Jones SM, Petit C. Otoferlin is critical for a highly sensitive and linear calcium-dependent exocytosis at vestibular hair cell ribbon synapses. J Neurosci. 2009 Aug 26;29(34):10474-87. doi: 10.1523/JNEUROSCI.1009-09.2009. PMID: 19710301; PMCID: PMC2966717.

- Eatock RA, Hurley KM. Functional development of hair cells. Curr Top Dev Biol. 2003; 57:389-448. doi: 10.1016/s0070-2153(03)57013-2. PMID: 14674488.

- Eatock RA, Rüsch A. Developmental changes in the physiology of hair cells. Semin Cell Dev Biol. 1997 Jun;8(3):265-275. doi: 10.1006/scdb.1997.0142. PMID: 10024489.

- Eatock RA, Songer JE. Vestibular hair cells and afferents: two channels for head motion signals. Annu Rev Neurosci. 2011; 34:501-34. doi: 10.1146/annurev-neuro-061010-113710. PMID: 21469959.

- Eatock RA. Adaptation in hair cells. Annu Rev Neurosci. 2000; 23:285-314. doi: 10.1146/annurev.neuro.23.1.285. PMID: 10845066.

- Eatock RA. Specializations for Fast Signaling in the Amniote Vestibular Inner Ear. Integr Comp Biol. 2018 Aug 1;58(2):341-350. doi: 10.1093/icb/icy069. PMID: 29920589; PMCID: PMC6104706.

- Fettiplace R, Hackney CM. The sensory and motor roles of auditory hair cells. Nat Rev Neurosci. 2006 Jan;7(1):19-29. doi: 10.1038/nrn1828. PMID: 16371947.

- Fettiplace R, Kim KX. The physiology of mechanoelectrical transduction channels in hearing. Physiol Rev. 2014 Jul;94(3):951-86. doi: 10.1152/physrev.00038.2013. PMID: 24987009; PMCID: PMC4101631.

- Fettiplace R. Defining features of the hair cell mechanoelectrical transducer channel. Pflugers Arch. 2009 Oct;458(6):1115-23. doi: 10.1007/s00424-009-0683-x. Epub 2009 May 28. PMID: 19475417; PMCID: PMC2745616.

- Fettiplace R. Hair Cell Transduction, Tuning, and Synaptic Transmission in the Mammalian Cochlea. Compr Physiol. 2017 Sep 12;7(4):1197-1227. doi: 10.1002/cphy.c160049. PMID: 28915323; PMCID: PMC5658794.

- Frank T, Khimich D, Neef A, Moser T. Mechanisms contributing to synaptic Ca^{2+} signals and their heterogeneity in hair cells. Proc Natl Acad Sci U S A. 2009 Mar 17;106(11):4483-8. doi: 10.1073/pnas.0813213106. Epub 2009 Feb 25. PMID: 19246382; PMCID: PMC2657422.

- Frank T, Rutherford MA, Strenzke N, Neef A, Pangršič T, Khimich D, Fejtova A, Gundelfinger ED, Liberman MC, Harke B, Bryan KE, Lee A, Egner A, Riedel D, Moser T. Bassoon and the synaptic ribbon organize Ca^{2+} channels and vesicles to add release sites and promote refilling. Neuron. 2010 Nov 18;68(4):724-38. doi: 10.1016/j.neuron.2010.10.027. Erratum in: Neuron. 2010 Dec 22;68(6):1202. Fetjova, Anna [corrected to Fejtova, Anna]. PMID: 21092861; PMCID: PMC3005353.

- Furness DN and Hackney CM. The structure and composition of the stereociliary bundle of vertebrate hair cells. 2006 In: Eatock RA, Fay RR and Popper AN (eds) Vertebrate Hair Cells. New York: Springer, 95-153.

- Furness DN, Katori Y, Nirmal Kumar B, Hackney CM. The dimensions and structural attachments of tip links in mammalian cochlear hair cells and the effects of exposure to different levels of extracellular calcium. Neuroscience. 2008 Jun 12;154(1):10-21. doi: 10.1016/j.neuroscience.2008.02.010. Epub 2008 Feb 19. PMID: 18384968.

- Gale JE and Jagger DJ. Cochlear supporting cells. 2010 In: Fuchs, P.A. (Ed.). The Oxford Handbook of Auditory Science: The Ear. Oxford University Press, Oxford; New York.

- Géléoc GS, Risner JR, Holt JR. Developmental acquisition of voltage-dependent conductances and sensory signaling in hair cells of the embryonic mouse inner ear. J Neurosci. 2004 Dec 8;24(49):11148-59. doi: 10.1523/JNEUROSCI.2662-04.2004. PMID: 15590931; PMCID: PMC2638092.

- Gerard J. Tortora and Mark T. Nielsen 2017. Priciple of Human Anatomy United States of America. Fourteenth edition.

- Giese APJ, Tang YQ, Sinha GP, Bowl MR, Goldring AC, Parker A, Freeman MJ, Brown SDM, Riazuddin S, Fettiplace R, Schafer WR, Frolenkov GI, Ahmed ZM. CIB2 interacts with TMC1 and TMC2 and is essential for mechanotransduction in auditory hair cells. Nat Commun. 2017 Jun 29;8(1):43. doi: 10.1038/s41467-017-00061-1. PMID: 28663585; PMCID: PMC5491523.

- Gillespie PG, Cyr JL. Myosin-1c, the hair cell's adaptation motor. Annu Rev Physiol. 2004; 66:521-45. doi: 10.1146/annurev.physiol.66.032102.112842. PMID: 14977412.

- Glowatzki E, Fuchs PA. Cholinergic synaptic inhibition of inner hair cells in the neonatal mammalian cochlea. Science. 2000 Jun 30;288(5475):2366-8. doi: 10.1126/science.288.5475.2366. PMID: 10875922.

- Glowatzki E, Fuchs PA. Transmitter release at the hair cell ribbon synapse. Nat Neurosci. 2002 Feb;5(2):147-54. doi: 10.1038/nn796. PMID: 11802170.

- Glowatzki E, Grant L, Fuchs P. Hair cell afferent synapses. Curr Opin Neurobiol. 2008 Aug;18(4):389-95. doi: 10.1016/j.conb.2008.09.006. Epub 2008 Oct 8. PMID: 18824101; PMCID: PMC2860955.

- Goldberg JM, Fernández C. Responses of peripheral vestibular neurons to angular and linear accelerations in the squirrel monkey. Acta Otolaryngol. 1975 Jul-Aug;80(1-2):101-10. doi: 10.3109/00016487509121307. PMID: 809987.

- Goldberg JM. The vestibular end organs: morphological and physiological diversity of afferents. Curr Opin Neurobiol. 1991 Aug;1(2):229-35. doi: 10.1016/0959-4388(91)90083-j. PMID: 1821186.

- Goodyear RJ, Marcotti W, Kros CJ, Richardson GP. Development and properties of stereociliary link types in hair cells of the mouse cochlea. J Comp Neurol. 2005 Apr 25;485(1):75-85. doi: 10.1002/cne.20513. PMID: 15776440.

- Goutman JD, Glowatzki E. Time course and calcium dependence of transmitter release at a single ribbon synapse. Proc Natl Acad Sci U S A. 2007 Oct 9;104(41):16341-6. doi: 10.1073/pnas.0705756104. Epub 2007 Oct 2. PMID: 17911259; PMCID: PMC2042208.

- Grabner CP, Moser T. Individual synaptic vesicles mediate stimulated exocytosis from cochlear inner hair cells. Proc Natl Acad Sci U S A. 2018 Dec 11;115(50):12811-12816. doi: 10.1073/pnas.1811814115. Epub 2018 Nov 21. PMID: 30463957; PMCID: PMC6294930.

- Grant L, Yi E, Glowatzki E. Two modes of release shape the postsynaptic response at the inner hair cell ribbon synapse. J Neurosci. 2010 Mar 24;30(12):4210-20. doi: 10.1523/JNEUROSCI.4439-09.2010. PMID: 20335456; PMCID: PMC2860956.

- Graydon CW, Cho S, Li GL, Kachar B, von Gersdorff H. Sharp Ca^{2+} nanodomains beneath the ribbon promote highly synchronous multivesicular release at hair cell synapses. J Neurosci. 2011 Nov 16;31(46):16637-50. doi: 10.1523/JNEUROSCI.1866-11.2011. PMID: 22090491; PMCID: PMC3235473.

- Griguer C, Sans A, Lehouelleur J. Non-typical K^{+}-current in cesium-loaded guinea pig type I vestibular hair cell. Pflugers Arch. 1993 Jan;422(4):407-9. doi: 10.1007/BF00374300. PMID: 8437892.

- Hackney CM, Furness DN. The composition and role of cross links in mechanoelectrical transduction in vertebrate sensory hair cells. J Cell Sci. 2013 Apr 15;126(Pt 8):1721-31. doi: 10.1242/jcs.106120. Epub 2013 May 2. PMID: 23641064.

- He DZ, Evans BN, Dallos P. First appearance and development of electromotility in neonatal gerbil outer hair cells. Hear Res. 1994 Jul;78(1):77-90. doi: 10.1016/0378-5955(94)90046-9. PMID: 7961180.

- Hille, B. 2001. Ion Channels of Excitable Membranes. Sinauer Associates, Inc. Sunderland, Massachusetts USA, Third Edition.

- Holt JC, Chatlani S, Lysakowski A, Goldberg JM. Quantal and nonquantal transmission in calyx-bearing fibers of the turtle posterior crista. J Neurophysiol. 2007 Sep;98(3):1083-101. doi: 10.1152/jn.00332.2007. Epub 2007 Jun 27. PMID: 17596419; PMCID: PMC3397384.

- Horwitz GC, Risner-Janiczek JR, Jones SM, Holt JR. HCN channels expressed in the inner ear are necessary for normal balance function. J Neurosci. 2011 Nov 16;31(46):16814-25. doi: 10.1523/JNEUROSCI.3064-11.2011. PMID: 22090507; PMCID: PMC3477615.

- Housley GD, Ashmore JF. Ionic currents of outer hair cells isolated from the guinea-pig cochlea. J Physiol. 1992 Mar; 448:73-98. doi: 10.1113/jphysiol. 1992. sp019030. PMID: 1593487; PMCID: PMC1176188.

- Hurley KM, Gaboyard S, Zhong M, Price SD, Wooltorton JR, Lysakowski A, Eatock RA. M-like K^+ currents in type I hair cells and calyx afferent endings of the developing rat utricle. J Neurosci. 2006 Oct 4;26(40):10253-69. doi: 10.1523/JNEUROSCI.2596-06.2006. PMID: 17021181; PMCID: PMC6674627.

- Jean P, Lopez de la Morena D, Michanski S, Jaime Tobón LM, Chakrabarti R, Picher MM, Neef J, Jung S, Gültas M, Maxeiner S, Neef A, Wichmann C, Strenzke N, Grabner C, Moser T. The synaptic ribbon is critical for sound encoding at high rates and with temporal precision. Elife. 2018 Jan 12;7: e29275. doi: 10.7554/eLife.29275. PMID: 29328020; PMCID: PMC5794258.

- Jeng JY, Carlton AJ, Johnson SL, Brown SDM, Holley MC, Bowl MR, Marcotti W. Biophysical and morphological changes in inner hair cells and their efferent innervation in the ageing mouse cochlea. J Physiol. 2021 Jan;599(1):269-287. doi: 10.1113/JP280256. Epub 2020 Nov 17. PMID: 33179774; PMCID: PMC7612127.

- Jeng JY, Ceriani F, Hendry A, Johnson SL, Yen P, Simmons DD, Kros CJ, Marcotti W. Hair cell maturation is differentially regulated along the tonotopic axis of the mammalian cochlea. J Physiol. 2020a Jan;598(1):151-170. doi: 10.1113/JP279012. Epub 2019 Dec 21. PMID: 31661723; PMCID: PMC6972525.

- Jeng JY, Ceriani F, Olt J, Brown SDM, Holley MC, Bowl MR, Johnson SL, Marcotti W. Pathophysiological changes in inner hair cell ribbon synapses in the ageing mammalian cochlea. J Physiol. 2020b Oct;598(19):4339-4355. doi: 10.1113/JP280018. Epub 2020 Aug 16. PMID: 32710572; PMCID: PMC7612121.

- Jeng JY, Johnson SL, Carlton AJ, De Tomasi L, Goodyear RJ, De Faveri F, Furness DN, Wells S, Brown SDM, Holley MC, Richardson GP, Mustapha M, Bowl MR, Marcotti W. Age-related changes in the biophysical and morphological characteristics of mouse cochlear outer hair cells. J Physiol. 2020 Sep;598(18):3891-3910. doi: 10.1113/JP279795. Epub 2020 Jul 22. PMID: 32608086; PMCID: PMC7612122.

- Johnson SL, Adelman JP, Marcotti W. Genetic deletion of SK2 channels in mouse inner hair cells prevents the developmental linearization in the Ca^{2+} dependence of exocytosis. J Physiol. 2007 Sep 1;583(Pt 2):631-46. doi: 10.1113/jphysiol.2007.136630. Epub 2007 Jul 12. PMID: 17627990; PMCID: PMC2096744.

- Johnson SL, Franz C, Knipper M, Marcotti W. Functional maturation of the exocytotic machinery at gerbil hair cell ribbon synapses. J Physiol. 2009 Apr 15;587(Pt 8):1715-26. doi: 10.1113/jphysiol.2009.168542. Epub 2009 Feb 23. PMID: 19237422; PMCID: PMC2683959.

- Johnson SL, Kuhn S, Franz C, Ingham N, Furness DN, Knipper M, Steel KP, Adelman JP, Holley MC, Marcotti W. Presynaptic maturation in auditory hair cells requires a critical period of sensory-independent spiking activity. Proc Natl Acad Sci U S A. 2013 May 21;110(21):8720-5. doi: 10.1073/pnas.1219578110. Epub 2013 May 6. PMID: 23650376; PMCID: PMC3666720.

- Johnson SL, Marcotti W, Kros CJ. Increase in efficiency and reduction in Ca^{2+} dependence of exocytosis during development of mouse inner hair cells. J Physiol. 2005 Feb 15;563(Pt 1):177-91. doi: 10.1113/jphysiol.2004.074740. Epub 2004 Dec 21. PMID: 15613377; PMCID: PMC1665557.

- Johnson SL, Marcotti W. Biophysical properties of $Ca_v1.3$ calcium channels in gerbil inner hair cells. J Physiol. 2008 Feb 15;586(4):1029-42. doi: 10.1113/jphysiol.2007.145219. Epub 2008 Jan 3. PMID: 18174213; PMCID: PMC2268984.

- Jones SM, Jones TA. Genetics of peripheral vestibular dysfunction: lessons from mutant mouse strains. J Am Acad Audiol. 2014 Mar;25(3):289-301. doi: 10.3766/jaaa.25.3.8. PMID: 25032973; PMCID: PMC4310552.

- Jorgensen JM, Anderson T. On the structure of the avian maculae. 1973. Acta Zool (Stockh) 54:121–130.

- Jorgensen JM. The sensory epithelia of the inner ear of two turtles. 1974. Testudo graeca L. and Pseudemys scripta (Schoepff). Acta Zool (Stockh) 55:289–298.

- Kachar B, Parakkal M, Kurc M, Zhao Y, Gillespie PG. High-resolution structure of hair-cell tip links. Proc Natl Acad Sci U S A. 2000 Nov 21;97(24):13336-41. doi: 10.1073/pnas.97.24.13336. Erratum in: Proc Natl Acad Sci U S A. 2013 Jul 16;110(29):12155. PMID: 11087873; PMCID: PMC27225.

- Kandler K, Clause A, Noh J. Tonotopic reorganization of developing auditory brainstem circuits. Nat Neurosci. 2009 Jun;12(6):711-7. doi: 10.1038/nn.2332. Epub 2009 May 10. PMID: 19471270; PMCID: PMC2780022.

- Khan S, Chang R. Anatomy of the vestibular system: a review. NeuroRehabilitation. 2013;32(3):437-43. doi: 10.3233/NRE-130866. PMID: 23648598.

- Khimich D, Nouvian R, Pujol R, Tom Dieck S, Egner A, Gundelfinger ED, Moser T. Hair cell synaptic ribbons are essential for synchronous auditory signalling. Nature. 2005 Apr 14;434(7035):889-94. doi: 10.1038/nature03418. PMID: 15829963.

- Kingma H, van de Berg R. Anatomy, physiology, and physics of the peripheral vestibular system. Handb Clin Neurol. 2016; 137:1-16. doi: 10.1016/B978-0-444-63437-5.00001-7. PMID: 27638059.

- Kollmar R, Montgomery LG, Fak J, Henry LJ, Hudspeth AJ. Predominance of the alpha1D subunit in L-type voltage-gated Ca^{2+} channels of hair cells in the chicken's cochlea. Proc Natl Acad Sci U S A. 1997 Dec 23;94(26):14883-8. doi: 10.1073/pnas.94.26.14883. PMID: 9405708; PMCID: PMC25132.

- Kollmar R, Montgomery LG, Fak J, Henry LJ, Hudspeth AJ. Predominance of the alpha1D subunit in L-type voltage-gated Ca^{2+} channels of hair cells in the chicken's cochlea. Proc Natl Acad Sci U S A. 1997a Dec 23;94(26):14883-8. doi: 10.1073/pnas.94.26.14883. PMID: 9405708; PMCID: PMC25132.

- Koschak A, Reimer D, Huber I, Grabner M, Glossmann H, Engel J, Striessnig J. alpha 1D ($Ca_v1.3$) subunits can form l-type Ca^{2+} channels activating at negative voltages. J Biol Chem. 2001 Jun 22;276(25):22100-6. doi: 10.1074/jbc.M101469200. Epub 2001 Apr 2. PMID: 11285265.

- Kros CJ, Marcotti W, van Netten SM, Self TJ, Libby RT, Brown SD, Richardson GP, Steel KP. Reduced climbing and increased slipping adaptation in cochlear hair cells of mice with Myo7a mutations. Nat Neurosci. 2002 Jan;5(1):41-7. doi: 10.1038/nn784. PMID: 11753415.

- Kros CJ, Ruppersberg JP, Rüsch A. Expression of a potassium current in inner hair cells during development of hearing in mice. Nature. 1998 Jul 16;394(6690):281-4. doi: 10.1038/28401. PMID: 9685158.

- Li GQ, Meredith FL, Rennie KJ. Development of K^+ and Na^+ conductances in rodent postnatal semicircular canal type I hair cells. Am J Physiol Regul Integr Comp Physiol. 2010 Feb;298(2): R351-8. doi: 10.1152/ajpregu.00460.2009. Epub 2009 Nov 25. PMID: 19939976; PMCID: PMC2828173.

- Liberman MC, Dodds LW, Pierce S. Afferent and efferent innervation of the cat cochlea: quantitative analysis with light and electron microscopy. J Comp Neurol. 1990 Nov 15;301(3):443-60. doi: 10.1002/cne.903010309. Erratum in: J Comp Neurol 1991 Feb 8;304(2):341. PMID: 2262601.

- Lim R, Kindig AE, Donne SW, Callister RJ, Brichta AM. Potassium accumulation between type I hair cells and calyx terminals in mouse crista. Exp Brain Res. 2011 May;210(3-4):607-21. doi: 10.1007/s00221-011-2592-4. Epub 2011 Feb 25. PMID: 21350807.

- Lindeman HH. Anatomy of the otolith organs. Adv Otorhinolaryngol. 1973; 20:405-33. doi: 10.1159/000393113. PMID: 4267996.

- Lysakowski A. Synaptic organization of the crista ampullaris in vertebrates. Ann N Y Acad Sci. 1996 Jun 19; 781:164-82. doi: 10.1111/j.1749-6632. 1996. Tb 15700.x. PMID: 8694413.

- Lysakowski A, Goldberg JM. 2004. The Vestibular System (57-152) Springer, New York, NY.

- Maeda R, Kindt KS, Mo W, Morgan CP, Erickson T, Zhao H, Clemens-Grisham R, Barr-Gillespie PG, Nicolson T. Tip-link protein protocadherin 15 interacts with transmembrane channel-like proteins TMC1 and TMC2. Proc Natl Acad Sci U S A. 2014 Sep 2;111(35):12907-12. doi: 10.1073/pnas.1402152111. Epub 2014 Aug 11. PMID: 25114259; PMCID: PMC4156717.

- Marcotti, Walter; and Masetto, Sergio 2010 Hair Cells. In: Encyclopedia of Life Sciences (ELS). John Wiley & Sons, Ltd: Chichester. doi: 10.1002/9780470015902.a0000181.pub2.

- Marcotti W, Corns LF, Goodyear RJ, Rzadzinska AK, Avraham KB, Steel KP, Richardson GP, Kros CJ. The acquisition of mechano-electrical transducer current adaptation in auditory hair cells requires myosin VI. J Physiol. 2016 Jul 1;594(13):3667-81. doi: 10.1113/JP272220. Epub 2016 May 27. PMID: 27111754; PMCID: PMC4929313.

- Marcotti W, Géléoc GS, Lennan GW, Kros CJ. Transient expression of an inwardly rectifying potassium conductance in developing inner and outer hair cells along the mouse cochlea. Pflugers Arch. 1999 Dec;439(1-2):113-22. doi: 10.1007/s004249900157. PMID: 10651007.

- Marcotti W, Johnson SL, Holley MC, Kros CJ. Developmental changes in the expression of potassium currents of embryonic, neonatal and mature mouse inner hair cells. J Physiol. 2003 Apr 15;548(Pt 2):383-400. doi: 10.1113/jphysiol.2002.034801. Epub 2003 Feb 14. Erratum in: J Physiol. 2003 Aug 1;550(Pt 3):996. PMID: 12588897; PMCID: PMC2342842.

- Marcotti W, Johnson SL, Kros CJ. A transiently expressed SK current sustains and modulates action potential activity in immature mouse inner hair cells. J Physiol. 2004 Nov 1;560(Pt 3):691-708. doi: 10.1113/jphysiol.2004.072868. Epub 2004 Aug 26. PMID: 15331671; PMCID: PMC1665291.

- Marcotti W, Johnson SL, Kros CJ. Effects of intracellular stores and extracellular Ca^{2+} on Ca^{2+}-activated K^{+} currents in mature mouse inner hair cells. J Physiol. 2004 Jun 1;557(Pt 2):613-33. doi: 10.1113/jphysiol.2003.060137. Epub 2004 Apr 2. PMID: 15064328; PMCID: PMC1665097.

- Marcotti W, Johnson SL, Rusch A, Kros CJ. Sodium and calcium currents shape action potentials in immature mouse inner hair cells. J Physiol. 2003 Nov 1;552(Pt 3):743-61. doi: 10.1113/jphysiol.2003.043612. Epub 2003 Aug 22. PMID: 12937295; PMCID: PMC2343463.

- Marcotti W, Kros CJ. Developmental expression of the potassium current $I_{K,n}$ contributes to maturation of mouse outer hair cells. J Physiol. 1999 Nov 1;520 Pt 3(Pt 3):653-60. doi: 10.1111/j.1469-7793.1999.00653.x. PMID: 10545133; PMCID: PMC2269630.

- Marcotti W. Functional assembly of mammalian cochlear hair cells. Exp Physiol. 2012 Apr;97(4):438-51. doi: 10.1113/expphysiol.2011.059303. Epub 2011 Dec 5. PMID: 22143883; PMCID: PMC3490375.

- Masetto S, Perin P, Malusà A, Zucca G, Valli P. Membrane properties of chick semicircular canal hair cells in situ during embryonic development. J Neurophysiol. 2000 May;83(5):2740-56. doi: 10.1152/jn.2000.83.5.2740. PMID: 10805673.

- Masetto S, Zampini V, Zucca G, Valli P. Ca^{2+} currents and voltage responses in Type I and Type II hair cells of the chick embryo semicircular canal. Pflugers Arch. 2005 Nov;451(2):395-408. doi: 10.1007/s00424-005-1466-7. Epub 2005 Aug 16. PMID: 16133262.

- Matthews G, Fuchs P. The diverse roles of ribbon synapses in sensory neurotransmission. Nat Rev Neurosci. 2010 Dec;11(12):812-22. doi: 10.1038/nrn2924. Epub 2010 Nov 3. PMID: 21045860; PMCID: PMC3065184.

- Meredith FL, Rennie KJ. Channeling your inner ear potassium: K^+ channels in vestibular hair cells. Hear Res. 2016 Aug; 338:40-51. doi: 10.1016/j.heares.2016.01.015. Epub 2016 Feb 4. PMID: 26836968.

- Mescher AL. Junqueira's Basic Histology: Text and Atlas. 2011. 12th Edition. Lange.

- Meyer AC, Frank T, Khimich D, Hoch G, Riedel D, Chapochnikov NM, Yarin YM, Harke B, Hell SW, Egner A, Moser T. Tuning of synapse number, structure and function in the cochlea. Nat Neurosci. 2009 Apr;12(4):444-53. doi: 10.1038/nn.2293. Epub 2009 Mar 8. PMID: 19270686.

- Michna M, Knirsch M, Hoda JC, Muenkner S, Langer P, Platzer J, Striessnig J, Engel J. $Ca_v1.3$ (alpha1D) Ca^{2+} currents in neonatal outer hair cells of mice. J Physiol. 2003 Dec 15;553(Pt 3):747-58. doi: 10.1113/jphysiol.2003.053256. Epub 2003 Sep 26. PMID: 14514878; PMCID: PMC2343630.

- Monzack EL, Cunningham LL. Lead roles for supporting actors: critical functions of inner ear supporting cells. Hear Res. 2013 Sep; 303:20-9. doi: 10.1016/j.heares.2013.01.008. Epub 2013 Jan 21. PMID: 23347917; PMCID: PMC3648608.

- Moser T, Beutner D. Kinetics of exocytosis and endocytosis at the cochlear inner hair cell afferent synapse of the mouse. Proc Natl Acad Sci U S A. 2000 Jan 18;97(2):883-8. doi: 10.1073/pnas.97.2.883. PMID: 10639174; PMCID: PMC15425.

- Ohn TL, Rutherford MA, Jing Z, Jung S, Duque-Afonso CJ, Hoch G, Picher MM, Scharinger A, Strenzke N, Moser T. Hair cells use active zones with different voltage dependence of Ca^{2+} influx to decompose sounds into complementary neural codes. Proc Natl Acad Sci U S A. 2016 Aug 9;113(32): E4716-25. doi: 10.1073/pnas.1605737113. Epub 2016 Jul 26. PMID: 27462107; PMCID: PMC4987782.

- Oliver D, Knipper M, Derst C, Fakler B. Resting potential and submembrane calcium concentration of inner hair cells in the isolated mouse cochlea are set by KCNQ-type potassium channels. J Neurosci. 2003 Mar 15;23(6):2141-9. doi: 10.1523/JNEUROSCI.23-06-02141.2003. PMID: 12657673; PMCID: PMC6742048.

- Oswald S 2000. Functional Neuroscience. New York Inc., United States.

- Pack AK, Slepecky NB. Cytoskeletal and calcium-binding proteins in the mammalian organ of Corti: cell type-specific proteins displaying longitudinal and radial gradients. Hear Res. 1995 Nov;91(1-2):119-35. doi: 10.1016/0378-5955(95)00173-5. PMID: 8647714.

- Pangrsic T, Lasarow L, Reuter K, Takago H, Schwander M, Riedel D, Frank T, Tarantino LM, Bailey JS, Strenzke N, Brose N, Müller U, Reisinger E, Moser T. Hearing requires otoferlin-dependent efficient replenishment of synaptic vesicles in hair cells. Nat Neurosci. 2010 Jul;13(7):869-76. doi: 10.1038/nn.2578. Epub 2010 Jun 20. PMID: 20562868.

- Pangrsic T, Singer JH, Koschak A. Voltage-Gated Calcium Channels: Key Players in Sensory Coding in the Retina and the Inner Ear. Physiol Rev. 2018 Oct 1;98(4):2063-2096. doi: 10.1152/physrev.00030.2017. PMID: 30067155; PMCID: PMC6170976.

- Petit C, Richardson GP. Linking genes underlying deafness to hair-bundle development and function. Nat Neurosci. 2009 Jun;12(6):703-10. doi: 10.1038/nn.2330. Epub 2009 May 26. PMID: 19471269; PMCID: PMC3332156.

- Picher MM, Gehrt A, Meese S, Ivanovic A, Predoehl F, Jung S, Schrauwen I, Dragonetti AG, Colombo R, Van Camp G, Strenzke N, Moser T. Ca^{2+}-binding protein 2 inhibits Ca^{2+}-channel inactivation in mouse inner hair cells. Proc Natl Acad Sci U S A. 2017 Feb 28;114(9): E1717-E1726. doi: 10.1073/pnas.1617533114. Epub 2017 Feb 9. PMID: 28183797; PMCID: PMC5338518.

- Pickles JO 2008. An Introduction to the Physiology of Hearing. Academic Press.

- Platzer J, Engel J, Schrott-Fischer A, Stephan K, Bova S, Chen H, Zheng H, Striessnig J. Congenital deafness and sinoatrial node dysfunction in mice lacking class D L-type Ca^{2+} channels. Cell. 2000 Jul 7;102(1):89-97. doi: 10.1016/s0092-8674(00)00013-1. PMID: 10929716.

- Poppi LA, Tabatabaee H, Drury HR, Jobling P, Callister RJ, Migliaccio AA, Jordan PM, Holt JC, Rabbitt RD, Lim R, Brichta AM. ACh-induced hyperpolarization and decreased resistance in mammalian type II vestibular hair cells. J Neurophysiol. 2018 Jan 1;119(1):312-325. doi: 10.1152/jn.00030.2017. Epub 2017 Oct 4. Erratum in: J Neurophysiol. 2018 Jul 1;120(1):385. PMID: 28978760; PMCID: PMC6048467.

- Pujol R, Puel JL. Excitotoxicity, synaptic repair, and functional recovery in the mammalian cochlea: a review of recent findings. Ann N Y Acad Sci. 1999 Nov 28; 884:249-54. doi: 10.1111/j.1749-6632. 1999. tb08646.x. PMID: 10842598.

- Rennie KJ, Correia MJ. Effects of cationic substitutions on delayed rectifier current in type I vestibular hair cells. J Membr Biol. 2000 Jan 15;173(2):139-48. doi: 10.1007/s002320001015. PMID: 10630929.

- Rennie KJ, Correia MJ. Potassium currents in mammalian and avian isolated type I semicircular canal hair cells. J Neurophysiol. 1994 Jan;71(1):317-29. doi: 10.1152/jn.1994.71.1.317. PMID: 8158233.

- Rennie KJ, Correia MJ. Potassium currents in mammalian and avian isolated type I semicircular canal hair cells. J Neurophysiol. 1994 Jan;71(1):317-29. doi: 10.1152/jn.1994.71.1.317. PMID: 8158233.

- Revenu C, Athman R, Robine S, Louvard D. The co-workers of actin filaments: from cell structures to signals. Nat Rev Mol Cell Biol. 2004 Aug;5(8):635-46. doi: 10.1038/nrm1437. PMID: 15366707.

- Rosenhall U. Some morphological principles of the vestibular maculae in birds. Arch Klin Exp Ohren Nasen Kehlkopfheilkd. 1970;197(2):154-82. doi: 10.1007/BF00306164. PMID: 4097821.

- Roux I, Safieddine S, Nouvian R, Grati M, Simmler MC, Bahloul A, Perfettini I, Le Gall M, Rostaing P, Hamard G, Triller A, Avan P, Moser T, Petit C. Otoferlin, defective in a human deafness form, is essential for exocytosis at the auditory ribbon synapse. Cell. 2006 Oct 20;127(2):277-89. doi: 10.1016/j.cell.2006.08.040. PMID: 17055430.

- Rüsch A, Eatock RA. A delayed rectifier conductance in type I hair cells of the mouse utricle. J Neurophysiol. 1996 Aug;76(2):995-1004. doi: 10.1152/jn.1996.76.2.995. PMID: 8871214.

- Safieddine S, El-Amraoui A, Petit C. The auditory hair cell ribbon synapse: from assembly to function. Annu Rev Neurosci. 2012; 35:509-28. doi: 10.1146/annurev-neuro-061010-113705. PMID: 22715884.

- Saladin, Kenneth S. 2017. Human Anatomy. Georgia College and State University. Fifth Edition.

- Schneider ME, Belyantseva IA, Azevedo RB, Kachar B. Rapid renewal of auditory hair bundles. Nature. 2002 Aug 22;418(6900):837-8. doi: 10.1038/418837a. PMID: 12192399.

- Schwander M, Kachar B, Müller U. Review series: The cell biology of hearing. J Cell Biol. 2010 Jul 12;190(1):9-20. doi: 10.1083/jcb.201001138. PMID: 20624897; PMCID: PMC2911669.

- Shnerson A, Devigne C, Pujol R. Age-related changes in the C57BL/6J mouse cochlea. II. Ultrastructural findings. Brain Res. 1981 Aug;254(1):77-88. doi: 10.1016/0165-3806(81)90060-2. PMID: 7272774.

- Simmons DD, Mansdorf NB, Kim JH. Olivocochlear innervation of inner and outer hair cells during postnatal maturation: evidence for a waiting period. J Comp Neurol. 1996 Jul 8;370(4):551-62. doi: 10.1002/(SICI)1096-9861(19960708)370:4<551:AID-CNE10>3.0.CO;2-M. PMID: 8807454.

- Söllner C, Rauch GJ, Siemens J, Geisler R, Schuster SC, Müller U, Nicolson T; Tübingen 2000 Screen Consortium. Mutations in cadherin 23 affect tip links in zebrafish sensory hair cells. Nature. 2004 Apr 29;428(6986):955-9. doi: 10.1038/nature02484. Epub 2004 Mar 31. PMID: 15057246.

- Songer JE, Eatock RA. Tuning and timing in mammalian type I hair cells and calyceal synapses. J Neurosci. 2013 Feb 20;33(8):3706-24. doi: 10.1523/JNEUROSCI.4067-12.2013. PMID: 23426697; PMCID: PMC3857958.

- Spaiardi P, Marcotti W, Masetto S, Johnson SL. Exocytosis in mouse vestibular Type II hair cells shows a high-order Ca^{2+} dependence that is independent of synaptotagmin-4. Physiol Rep. 2020b Jul;8(14): e14509. doi: 10.14814/phy2.14509. PMID: 32691536; PMCID: PMC7371649.

- Spaiardi P, Tavazzani E, Manca M, Milesi V, Russo G, Prigioni I, Marcotti W, Magistretti J, Masetto S. An allosteric gating model recapitulates the biophysical properties of $I_{K,L}$ expressed in mouse vestibular type I hair cells. J Physiol. 2017 Nov 1;595(21):6735-6750. doi: 10.1113/JP274202. Epub 2017 Sep 24. PMID: 28862328; PMCID: PMC5663832.

- Spaiardi P, Tavazzani E, Manca M, Russo G, Prigioni I, Biella G, Giunta R, Johnson SL, Marcotti W, Masetto S. K^+ Accumulation and Clearance in the Calyx Synaptic Cleft of Type I Mouse Vestibular Hair Cells. Neuroscience. 2020a Feb 1; 426:69-86. doi: 10.1016/j.neuroscience.2019.11.028. Epub 2019 Dec 14. PMID: 31846752; PMCID: PMC6985899.

- Spitzmaul G, Tolosa L, Winkelman BH, Heidenreich M, Frens MA, Chabbert C, de Zeeuw CI, Jentsch TJ. Vestibular role of KCNQ4 and KCNQ5 K^+ channels revealed by mouse models. J Biol Chem. 2013 Mar 29;288(13):9334-44. doi: 10.1074/jbc.M112.433383. Epub 2013 Feb 13. PMID: 23408425; PMCID: PMC3611004.

- Wersall J, Bagger-Sjoback D. Morphology of the vestibular sense organ. 1974. In: Kornhuber HH (ed) Handbook of Sensory Physiology. Vestibular System. Basic Mechanisms. New York: Springer, pp. 123–170.

- Wooltorton JR, Gaboyard S, Hurley KM, Price SD, Garcia JL, Zhong M, Lysakowski A, Eatock RA. Developmental changes in two voltage-dependent sodium currents in utricular hair cells. J Neurophysiol. 2007 Feb;97(2):1684-704. doi: 10.1152/jn.00649.2006. Epub 2006 Oct 25. PMID: 17065252.

- Xu W, Lipscombe D. Neuronal Ca(V)1.3 alpha (1) L-type channels activate at relatively hyperpolarized membrane potentials and are incompletely inhibited by dihydropyridines. J Neurosci. 2001 Aug 15;21(16):5944-51. doi: 10.1523/JNEUROSCI.21-16-05944.2001. PMID: 11487617; PMCID: PMC6763157.

- Yamashita M, Ohmori H. Synaptic responses to mechanical stimulation in calyceal and bouton type vestibular afferents studied in an isolated preparation of semicircular canal ampullae of chicken. Exp Brain Res. 1990;80(3):475-88. doi: 10.1007/BF00227989. PMID: 2387349.

- Zampini V, Johnson SL, Franz C, Knipper M, Holley MC, Magistretti J, Masetto S, Marcotti W. Burst activity and ultrafast activation kinetics of $Ca_v1.3$ Ca^{2+} channels support presynaptic activity in adult gerbil hair cell ribbon synapses. J Physiol. 2013 Aug 15;591(16):3811-20. doi: 10.1113/jphysiol.2013.251272. Epub 2013 May 27. PMID: 23713031; PMCID: PMC3764630.

- Zampini V, Johnson SL, Franz C, Knipper M, Holley MC, Magistretti J, Russo G, Marcotti W, Masetto S. Fine Tuning of $Ca_V1.3$ Ca^{2+} channel properties in adult inner hair cells positioned in the most sensitive region of the Gerbil Cochlea. PLoS One. 2014 Nov 19;9(11): e113750. doi: 10.1371/journal.pone.0113750. PMID: 25409445; PMCID: PMC4237458.

- Zidanic M, Fuchs PA. Kinetic analysis of barium currents in chick cochlear hair cells. Biophys J. 1995 Apr;68(4):1323-36. doi: 10.1016/S0006-3495(95)80305-X. PMID: 7787021; PMCID: PMC1282027.

Sitography

https://images.app.goo.gl/C7i98SyvYN3bwp4V8
https://open.oregonstate.education/aandp/chapter/15-4-equilibrium/
https://images.app.goo.gl/NigBU7V5LisBxNcW8
https://mutagenetix.utsouthwestern.edu/phenotypic/phenotypic_rec.cfm?pk=1299
https://lab.research.sickkids.ca/harrison